iScience

Article

Targeting G9a-m^{6}A translational mechanism of SARS-CoV-2 pathogenesis for multifaceted therapeutics of COVID-19 and its sequalae

Graphical abstract

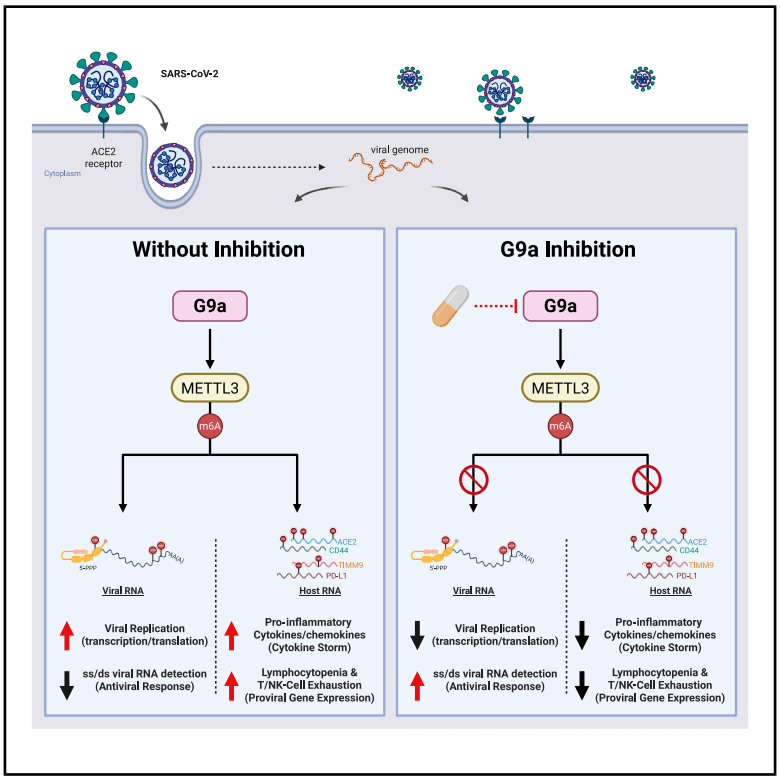

Highlights

- G9a interacts with translation regulators to promote turnover of proviral factors
- G9a-METTL3-m^{6}A axis rewires viral/host m^{6}A methylome following SARS-CoV-2 infection
- G9a regulates poised-mRNA expression in COVID-19 patient PBMCs and autopsy samples
- G9a/Ezh2 inhibition reverses multi-omic landscape of SARS-CoV-2 infection

Authors

Adil Muneer, Ling Xie, Xuping Xie, ..., Hongjun Song, Pei-Yong Shi, Xian Chen

Correspondence

xianc@email.unc.edu

In brief

Natural sciences; Biological sciences; Microbiology; Virology

Muneer et al., 2025, iScience *28*, 112632
June 20, 2025
https://doi.org/10.1016/j.isci.2025.112632

CellPress

iScience

CellPress
OPEN ACCESS

Article

Targeting G9a-m^{6}A translational mechanism of SARS-CoV-2 pathogenesis for multifaceted therapeutics of COVID-19 and its sequalae

Adil Muneer,[1,10] Ling Xie,[1,10] Xuping Xie,[3,9] Feng Zhang,[4] John A. Wrobel,[1] Yan Xiong,[5] Xufen Yu,[5] Charles Wang,[6] Ciprian Gheorghe,[6] Ping Wu,[7] Juan Song,[8] Guo-Li Ming,[4] Jian Jin,[5] Hongjun Song,[4] Pei-Yong Shi,[3,7,9] and Xian Chen[1,2,11,*]

[1]Department of Biochemistry & Biophysics, University of North Carolina at Chapel Hill, Chapel Hill, NC 27599, USA
[2]Lineberger Comprehensive Cancer Center, University of North Carolina at Chapel Hill, Chapel Hill, NC 27599, USA
[3]Department of Biochemistry and Molecular Biology, University of Texas Medical Branch, Galveston, TX, USA
[4]Department of Neuroscience and Mahoney Institute for Neurosciences, University of Pennsylvania, Philadelphia, PA 19104, USA
[5]Mount Sinai Center for Therapeutics Discovery, Departments of Pharmacological Sciences, Oncological Sciences, and Neuroscience, Tisch Cancer Institute, Icahn School of Medicine at Mount Sinai, New York, NY 10029, USA
[6]Center for Genomics, Division of Microbiology & Molecular Genetics, Department of Basic Sciences, Lawrence D Longo MD Center for Perinatal Biology, Department of Gynecology and Obstetrics, School of Medicine, Loma Linda University, Loma Linda, CA 92350, USA
[7]Department of Neuroscience, Cell Biology, and Anatomy, Center for Addiction Sciences and Therapeutics, Brain Health Institute, Mitchell Center for Neurodegenerative Diseases, University of Texas Medical Branch, Galveston, TX, USA
[8]Department of Pharmacology, and Neuroscience Center, University of North Carolina at Chapel Hill, Chapel Hill, NC 27599, USA
[9]Institute for Human Infections and Immunity, Sealy Institute for Vaccine Sciences, Sealy Center for Structural Biology & Molecular Biophysics, University of Texas Medical Branch, Galveston, TX, USA
[10]These authors contributed equally
[11]Lead contact
*Correspondence: xianc@email.unc.edu
https://doi.org/10.1016/j.isci.2025.112632

SUMMARY

N6-methyladenosine (m6A) modification pathway is hijacked by several RNA viruses, including SARS-CoV-2, making it an attractive host-directed target for development of broad-spectrum antivirals. Here, we show that histone methyltransferase G9a, through its interaction with METTL3, regulates SARS-CoV-2-mediated rewiring of host m6A methylome to ultimately promote turnover, abundance, secretion and/or phosphorylation of various viral receptors and proteases, transcription factors, cytokines/chemokines, coagulation and angiogenesis associated proteins, and fibrosis markers. More importantly, drugs targeting G9a and its associated protein EZH2 are potent inhibitors of SARS-CoV-2 replication and reverse multi-omic effects of coronavirus infection in human alveolar epithelial cells (A549-hACE2) and COVID-19 patient peripheral blood mononuclear cells (PBMCs)—with similar changes seen in multiorgan autopsy samples from COVID-19 patients. Altogether, we extend G9a function(s) beyond transcription to translational regulation during COVID-19 pathogenesis and show that targeting this master regulatory complex represents a new strategy (drug-class) that can be leveraged to combat emerging anti-viral resistance and infections.

INTRODUCTION

The coronavirus disease (COVID-19) pandemic, caused by severe acute respiratory syndrome coronavirus-2 (SARS-CoV-2), is an unprecedented global public health crisis having already claimed more than 6.8 million lives worldwide.[1] Particularly, high mortality is observed for SARS-CoV-2-infected patients who have pre-existing chronic conditions, such as recovery from sepsis, chronic pulmonary diseases, metabolic diseases (e.g., diabetes), asthma, cardiovascular diseases, thrombosis, chronic liver disease and cirrhosis, and cancer.[2,3] Despite initial success of vaccines in reducing COVID-19 infections, hospitalizations, and deaths, neutralizing antibody levels eventually wane with time[4,5] and genomic variation owing to low replication fidelity[6,7] leads to emergence of SARS-CoV-2 variants having increased transmissibility or virulence. For example, an Omicron subvariant, XBB.1.16, also known as Arcturus, has fueled a surge of COVID-19 cases in 2022.[8] Accordingly, none of the available monoclonal antibodies, with emergency use authorization, neutralize Omicron and its variants effectively.[9–11] Also, development of resistance has been observed for antiviral drugs that target either SARS-CoV-2 polymerase (e.g., Remdesivir, Molnupiravir) or protease (e.g., Paxlovid).[12–14] More importantly, without available clinical drugs, emerging cases of post-acute sequela of COVID-19 (aka "long COVID") have been reported.[15] For example, COVID-19 causes a plethora of neurological, neuropsychiatric, and psychological impairments, such as ischemic and hemorrhagic stroke, encephalopathy, encephalitis,

brain fog, depression, anxiety, and sleep disorders.[16] Yet, SARS-CoV-2 pathogenesis and the etiology of long COVID neurological symptoms are poorly understood. To effectively combat both emerging variants of the coronavirus and long-lasting COVID-19 sequelae, key mechanistic questions need to be answered, including (1) how SARS-CoV2 life cycle is regulated in the host, and (2) how SARS-CoV2 hijacks host pathways to promote COVID-19 pathogenesis.

The molecular/cellular hallmarks of COVID-19 pathogenesis include increased proportion of monocyte-derived macrophages, reduction and functional exhaustion of T cells (lymphopenia), and increased levels of serum cytokines (hyperinflammation)[17,18]; together, these circumstances result in sepsis and acute respiratory distress syndrome (ARDS), two leading complications associated with severe COVID-19.[19,20] In correlation with the crucial function of histone modification and chromatin remodeling during SARS-CoV-2 infection,[21] the histone methyltransferases G9a and G9a-like protein (GLP; hereafter G9a will represent both proteins) showed upregulated expression in COVID-19 patients who had high virus load.[22] In addition, in support of our indication of G9a inhibitor efficacy for multifaceted COVID-19 therapeutics[23,24] (US patent application #US18/035,831), Sakai et al. reported recently that treating SARS-CoV-2-infected hamsters with our G9a activity inhibitor UNC0642 not only suppressed SARS-CoV-2 replication but also mitigated infection-induced lung damage.[25] These results from the hamster infection model implicated G9a activity-associated pathways and mechanisms in COVID-19 pathogenesis. However, the well-understood canonical function of G9a in gene-specific transcriptional silencing did not explain how translation of other proteins was upregulated in the immunocompromised states of COVID-19.

Proteomic dissection of endogenous protein-protein interaction complexes (interactomes) has unique strengths for discovery of new functions of bait proteins, which can be extrapolated by identifying interactors that have known functions.[26,27] Because the systemic cytokine profiles in severe COVID-19 patients were similar to profiles in macrophage activation syndromes,[28] particularly viral sepsis,[19] we used our chromatin activity-based chemoproteomic (ChaC) technique with a biotinylated G9a inhibitor UNC0965[29] to dissect G9a-interacting pathways in the peripheral blood mononuclear cells (PBMCs) of COVID-19 patients. Notably, unlike conventional immunoprecipitation (IP)-MS[26,27] that characterizes protein complexes based only on epitope abundance, ChaC identified *in vivo* interactors of constitutively active G9a specifically from the diseased cells in the PBMCs with different cell types. Akin to endotoxin-tolerant (ET) macrophages[30] that have molecular characteristics similar to the immunopathological background of COVID-19 vulnerable groups that have pre-existing chronic inflammatory diseases,[17,18] UNC0965 ChaC-MS identified numerous regulators of translation, ribosome biogenesis, and proteostasis that had enhanced interaction with G9a in COVID-19 patient PBMCs. Coincidently, in the lungs of deceased COVID-19 patients, major protein translation pathways were found dysregulated.[31] In addition, in a recent study of virus-host protein interactome, Zhou et al. revealed that, via interactions with host translational regulators, SARS-CoV-2 hijacks the corresponding translational pathways.[32] Thus, our ChaC identification of G9a interaction with multiple regulators of SARS-CoV-2 hijacked translation now extends G9a activity beyond its transcriptional repression function to translational regulation of SARS-CoV-2 pathogenesis.

Specifically, in COVID-19 related samples, G9a-interacting translation regulators included the N^6-methyladenosine (m^6A) RNA methylase METTL3,[33,34] the ribosomal (r)RNA methylase fibrillarin (FBL), and another histone methyltransferase Ezh2. METTL3 is implicated in viral m^6A RNA modification and SARS-CoV2 dysregulated host immune response,[35–38] and elevated m^6A levels were found associated with severe clinical outcomes and mortality of COVID-19 patients.[39–42] SARS-CoV-2 can escape the host cell innate immune response by mimicking the host mRNA capping machinery and 2′-O methylation (2′-*O*-Me), the most prevalent modification in rRNA; FBL is the only known methyltransferase that catalyzes site-specific 2′-*O*-Me of rRNA. Importantly, Ezh2 and FBL, both of which interact with G9a, were found in a complex that regulates the 2′-*O*-Me rRNA-mediated protein synthesis.[43] The abovementioned reports in conjunction with our ChaC findings raised a triggering possibility that, via COVID-19-characteristic interactions with METTL3 or Ezh2/FBL, G9a coordinates m^6A- or Ezh2-mediated SARS-CoV-2 pathogenesis.

Like Bojkova et al. who found that viral replication was prevented by inhibitors of translation pathways reshaped by SARS-CoV-2,[44] we showed that inhibitors of G9a and Ezh2 (G9a interactor) suppressed viral replication in SARS-CoV-2 infected human alveolar epithelial cells that overexpressed human ACE2 (A549-hACE2). Combined, these results implicated the G9a interactome in regulating translation of virus growth in the host. On the basis of the *in vivo* effect of UNC0642 in reversing COVID-19 pathology,[25] we used G9a and Ezh2 inhibitors as the mechanistic probes to conduct multiomics analyses to investigate inhibitor effects on the SARS-CoV-2 infection-induced, G9a-related transcriptome, m^6A RNA epitranscriptome, proteome, phosphoproteome, and secretome of the A549-hACE2 cells or *ex vivo* culture of COVID-19 patient PBMCs. Correlations of these multiomics data showed that G9a inhibition reversed SARS-CoV-2-induced changes in m^6A RNA abundance and/or expression, phosphorylation, or secretion of specific proteins; these proteins whose translation was regulated by G9a (i.e., affected by G9a inhibitor) unite the networks associated with major stages of COVID-19 pathogenesis including host-virus interactions, and dysregulated host immune response. These results indicated that constitutively active G9a is the upstream/master regulator of widespread translational or post-translational (e.g., phosphorylation or secretion) processes associated with COVID-19 pathogenesis. Further, these results elucidated the mechanisms of inhibitor action toward both virus and the dysregulated host response that broadly reversed synthesis and degradation of specific proteins that ultimately define COVID-19 pathology. In correlation with the fact that abnormal m^6A modification enhances the replication of a broad range of coronaviruses/variants and their associated pathogenesis,[45,46] we found that G9a inhibition reversed the m^6A epitranscriptome landscape associated with SARS-CoV2 infection. These results implicated G9a inhibition in broad-spectrum blockade of

emerging coronavirus variants or any virus. In addition, we identified multiple G9a-regulated, inhibitor-reversed pathways characteristic of long COVID or COVID neurological symptoms. Importantly, akin to our finding that a brain-penetrant inhibitor of G9a, MS1262, reversed brain neuropathological pathways associated with Alzheimer's disease pathogenesis,[47] we found that MS1262 suppressed SARS-CoV2 replication, suggesting a therapeutic effect of G9a inhibition on long-lasting COVID neurological symptoms.

In sum, our COVID-19 pathology correlated multi-omics studies reveal a novel G9a-translation mechanism of COVID-19 pathogenesis from which we derived/validated biomarkers that can identify patient populations vulnerable to severe symptoms. Accordingly, targeting G9a and its interactor Ezh2 represents both virus- and host-directed therapeutics of severe COVID-19 and long COVID.

RESULTS

G9a activity-dependent interactome is implicated in the translational regulation of COVID-19 pathogenesis

To determine at which regulatory layer G9a promotes COVID-19 pathogenesis, we dissected G9a-associated pathways by our label-free quantitation (LFQ)[48] ChaC-MS approach. We used two ChaC probes, i.e., UNC0965 for G9a[29] and UNC2399 for Ezh2[49] for capturing G9a- and Ezh2-interacting complexes in the PBMCs from COVID-19 patients. For comparison, we included ChaC-MS results for G9a complexes obtained from ET macrophage cells[30] (Figure 1A). Three technical replicates were performed for each biological replicate, and principal-component analysis (PCA) showed good separation between G9a, EZH2, and control (UNC0125) pulldowns from patient PBMCs (Figure S1C). Based on LFQ ratios that are proportional to the relative binding of individual proteins to G9a or Ezh2 in COVID-19 patient PBMCs, LFQ ChaC-MS identified 1319 protein groups, of which 822 and 410 proteins were identified as G9a and Ezh2 interactors, respectively, in at least one COVID-19 patient, and 368 proteins were shared between the two methyltransferases. (Figures 1B and S1D; Table S1A). Unsurprisingly, there was significant overlap between G9a/Ezh2 interactors in COVID-19 patients and ET macrophages. In agreement with the canonical epigenetic (transcriptional) regulatory function of G9a and EZH2, we identified several proteins associated with chromatin remodeling and histone modification, including the SWI/SNF remodeling complex and BRD4, which were identified by siRNA and genome-wide CRISPR screens as essential host factors for SARS and pan-coronavirus infection, respectively[21,50] (Figures 1B and S1E). Similarly, in line with reports that core components of the G9a complex including EHMT1 and WIZ interact with SARS-CoV-2 encoded ORF9c,[51,52] we found 51 ChaC-identified interactors associated with ORF9c, and turnover of 24 other proteins was upregulated following infection[44] (Figure 1B; Table S1B), indicating the regulatory function of G9a interactome in COVID-19 immunopathogenesis.

In addition, ChaC revealed that G9a and Ezh2 interacted with the same translational regulators in ET macrophages and COVID-19 patient PBMCs (Figures 1B, 1C, and S1E). Notably, among the ChaC-identified G9a-interacting translation regulators, the splicing factor SF3B1 and the 40S ribosomal protein Rps14 were identified as patient PBMC- and ET-specific G9a interactors (Table S1B); Bojkova et al. showed that emetine inhibition of Rps14 and pladienolide inhibition of SF3B1 significantly reduced SARS-CoV-2 replication.[44] In correlation with the newly characterized function of EZH2 in translation regulation,[43] numerous members of the EZH2 complex were identified, such as EZH1, EZH2, EED, and SUZ12. Broadly, interactors shared between patient PBMC- or ET-macrophage specific G9a and EZH2 were primarily involved in translation elongation, immunity, angiogenesis and blood coagulation, cytoskeletal rearrangement, and vesicle-mediated transport—all pathways dysregulated by SARS-CoV-2 infection[18,19,22,44,53–55] (Figure 1C). These UNC0965 ChaC findings were highly correlated with COVID-19 clinicopathology because (1) in nasopharyngeal swabs and/or autopsy samples from severe COVID-19 patients, multiple G9a, EZH2, and METTL3 complex members are observed to be simultaneously dysregulated (Figures S1A and S1B), (2) histone mimicry by SARS-CoV-2 encoded ORF8 resulted in simultaneous increases of G9a- and Ezh2-catalyzed methylation at the histone H3 K9 and K27 following SARS-CoV-2 infection,[56,57] and (3) EZH2 binds METTL3[58] and EZH2 regulates IRES-dependent translation.[43] Taken together, these SARS-CoV-2 pathology-correlated findings of ChaC-MS suggested that, via interactions with host translation regulators, such as METTL3 and EZH2, SARS-CoV-2-upregulated G9a noncanonically function in the SARS-CoV-2 hijacked translational regulation of COVID immunopathogenesis.

G9a-interacting translation pathways promote SARS-CoV-2 infection and replication

In ET macrophages that mimic the immunopathological phenotype of COVID-19, we found[30] that G9a and METTL3 coregulated the m^{6}A-mediated translation of proteins associated with sepsis and ARDS complications of severe COVID-19.[19,20] Specifically, our translatome proteomics and m^{6}A RIP-Seq analysis of ET macrophages identified proteins whose translation was G9a-dependent ("G9a-translated" proteins); these proteins included 503 host interactors of SARS-CoV-1/2- and MERS-CoV-encoded proteins,[59,60] 11 known COVID-19 markers,[18,53] and 66 other coronavirus pathogenesis-related proteins (Figures 1D, S2A, and S2C; also see Table S1C). Certain G9a-translated proteins were ChaC-identified G9a interactors and/or non-histone G9a substrates and/or G9a/METTL3-coregulated m^{6}A targets in both patient PBMCs and ET macrophages (Figure 1D), which further supported the translational or post-translational function of G9a in COVID-19 pathogenesis. More importantly, genetic perturbation of numerous G9a-translated host interactors of SARS-CoV-1/2- and MERS-CoV-encoded proteins impairs SARS-CoV-2 replication and infection.[21,60] These G9a-translated, host-virus interactors were primarily involved in signaling pathways related to gene expression, cell cycle, immunity (e.g., leukocyte activation, neutrophil degranulation), translation (e.g., ribosome/ribonucleoprotein biogenesis), RNA processing (e.g., splicing and transport), and proteostasis (e.g., proteolysis, ubiquitination, autophagy, secretion, exocytosis, protein folding/localization/transport). In fact, all of these pathways are implicated in the SARS-CoV-2 life cycle and COVID-19 pathogenesis[18,19,22,44,53–55] (Figure 1D).

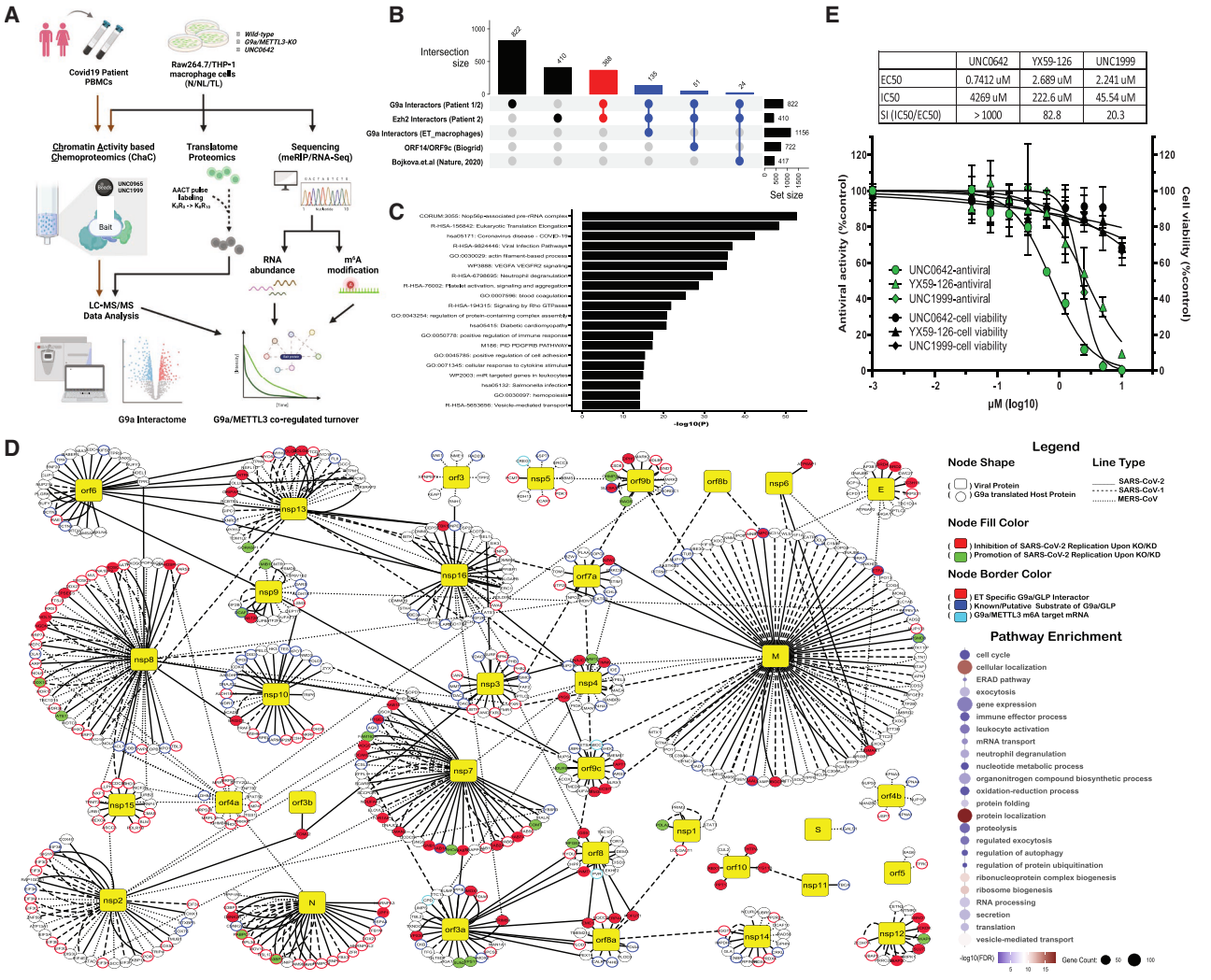

Figure 1. G9a interacts with host translation regulators to promote SARS-CoV-2 replication and proviral gene expression

(A) Schematic overview of multi-omics workflow to dissect function of G9a during COVID-19.

(B) Upset plot showing number of ChaC-identified G9a/EZH2 interactors in patient PBMCs or ET macrophage cells. Shared interactors are shown in red; in blue is shown interactor overlap with ChaC-MS results from ET macrophages, ORF14 host interactors, and proteins with SARS-CoV-2 upregulated turnover. The histogram on right shows the total number of hits in each dataset.

(C) Pathway enrichment results for 368 G9a/EZH2 shared interactors identified from patient PBMCs. *p* values were calculated based on the cumulative hypergeometric distribution followed by Benjamini-Hochberg procedure to account for multiple testing.

(D) Virus-host protein-protein interaction map depicting G9a-translated host interactors. Human proteins are shown as circles, whereas viral proteins are represented by yellow squares. Each edge represents an interaction between a human and a SARS-CoV-2 (solid line), SARS-CoV-1 (dashed line), or MERS-CoV (dotted line) encoded protein with certain interactions shared between these three viruses. Node border colors show ET/PBMC-specific G9a interactors that are, respectively, G9a-translated host proteins (red), G9a/GLP substrates (blue) or G9a/METTL3-coregulated m^{6}A modified mRNAs (cyan). Node fill color shows that genetic perturbation of several of these G9a-translated proteins hinders (red) or promotes (green) SARS-CoV-2 replication/infection. Pathway enrichment scores for 503 G9a translated host interactors, calculated using cumulative hypergeometric distribution followed by BH-procedure to account for multiple testing, are shown on the side. ET-specific G9a interactors and G9a/METTL3-coregulated m^{6}A targets were defined in ref.[25], whereas host-virus physical interactions, effects of genetic perturbation on SARS-CoV-2 replication/infection, and G9a/GLP substrate definitions were curated manually from literature sources.

(E) Antiviral activity (n = 2) and cytotoxicity (n = 3) of indicated compounds were evaluated in A549-hACE2 cells. Data are represented as mean ± SEM. Half-maximum effective concentration (EC_{50}) and cytotoxicity concentration (CC_{50}) values were calculated by fitting a nonlinear regression model (four parameters) with results summarized in table. (See also Figures S1 and S2; Table S1).

Similarly, several host factors critical for SARS-CoV-2 infection identified in siRNA/CRISPR-based screens are closely related to G9a complex[21,60] (Figure S2D). These results systematically revealed the associations of G9a interactome and G9a-translated proteins with host-virus interactions and SARS-CoV-2 infection/replication.

To validate the in vivo function of the G9a activity-dependent interactome in SARS-CoV-2 pathogenesis, we evaluated multiple

G9a- and EZH2-targeting compounds for their antiviral activity against SARS-CoV-2-Nluc in a human alveolar epithelial cell line that overexpresses human ACE2 receptor (A549-hACE2). Briefly, compounds targeting G9a including *UNC0642 (*EC_{50} = 0.74 μM; CC_{50} = 4269 μM; SI > 1000*) and* MS1262 (EC_{50} = 2.69 μM; CC_{50} = 223 μM; SI = 83) showed potent antiviral activity against SARS-CoV-2 with good selectivity indices (SI = CC_{50}/EC_{50}). Similarly, Ezh2 inhibitor *UNC1999* (EC_{50} = 2.241 μM; CC_{50} = 48.54 μM; SI = 20) hindered SARS-CoV-2 replication in this model system, whereas tazemetostat (EC_{50} = >10 μM; CC_{50} = >10 μM; SI = >1), a potent EZH2 inhibitor approved for treatment of epithelioid sarcoma and follicular lymphoma,[61] showed moderate decrease in virus proliferation (Figures 1E and S1F). Thus, drugs that target G9a or its interactor Ezh2 are potent suppressors of SARS-CoV-2 replication at sub/low micromolar concentrations and with good selectivity, making them attractive candidates for COVID-19 therapy.

SARS-CoV-2 and G9a co-regulate host response pathways primarily at the translational and post-translational levels

To further clarify G9a's function in the translational regulation of SARS-CoV-2 pathogenesis, we investigated G9a inhibitor effects on the SARS-CoV-2 infection-induced transcriptome, m^6A RNA epitranscriptome, proteome, phosphoproteome, and secretome. Correspondingly, we conducted COVID-19 pathology-correlated, multiomics analyses of SARS-CoV-2 infected A549-hACE2 cells or *ex vivo* culture of COVID-19 patient PBMCs with and without UNC0642 (a G9a inhibitor) treatment (Figures 2A and S3A). PCA showed clear separation between mock- and SARS-CoV-2 infected A549-hACE2 cells while, expectedly, UNC0642 treatment led to a distinct omics landscape compared with controls (Figure S3B). High reproducibility was observed between biological replicates and across experimental conditions across datasets (Figure S3C). In total, high-quality quantification for 49,021 human or viral entities, including 29,756 transcripts, 7,461 protein families, 11,217 phosphoproteins, and 587 secreted proteins, was obtained across datasets. There were 3,211 entries (1,393 RNA-seq, 109 proteome, 1,326 phospho-proteome, and 383 secretome) that showed differential enrichment for indicated comparisons (Figures S3D and S3E; Table S2). Effective infection of A549-hACE2 by SARS-CoV-2 was confirmed by a dramatic increase in viral transcripts and encoded proteins (Figure 2B).

After cellular entry mediated by receptors and proteases, SARS-CoV-2 hijacks host translation machinery to induce a hyper-inflammatory response mediated by particular transcriptional factors (TFs). This response leads to a ''cytokine-storm'' that is implicated in blood hypercoagulability, fibrosis, and micro-thrombosis in severe COVID-19 patients.[62,63] Correspondingly, we identified these process-related proteins that showed SARS-CoV-2-induced expression changes, including various viral receptors and proteases, TFs, cytokines (and their receptors), and proteins associated with coagulation, angiogenesis, and fibrosis (Figure S3E).

From a systems view, our multiomics-correlated data showed that SARS-CoV-2 infection led to activation of pathways related to (1) viral replication—including coronavirus replication and pathogenesis, phagocytosis, xenobiotic metabolism, and LPS-stimulated MAPK signaling, (2) host innate/adaptive immune response—encompassing the complement cascade, leukocyte extravasation, ILK, IFN, chemokine, NF-kB, CD40, CCR3, and JAK-STAT signaling, (3) coagulation and thrombosis—involving renin-angiotensin, VEGF, endothelin, thrombin, angiopoietin, and erythropoietin signaling, (4) protein translation—including PI3K/AKT, p70S6K/mTOR, EIF2, and ERK/MAPK signaling, (5) cellular homeostasis—involving autophagy, sirtuin signaling, the TCA cycle, and glycolysis, and (6) fibrosis—such as hepatic and idiopathic pulmonary fibrosis. (Figure 2C). In addition, gene ontology enrichment analysis revealed functional terms related to SARS infection, cell cycle, protein phosphorylation, growth factor signaling, and neutrophil/platelet degranulation (Figure S3F). In parallel, kinase activity scores estimated from quantitative phospho-proteomic data showed that SARS-CoV-2 infection leads to activation of several kinases including members of the p38/MAPK pathway (MAPK1, MAPK13, ERK, and ERBB3), CK1 (CSNK2A1), AKT/PI3K pathway (RSK and RPS6KA), Ca^{2+}/calmodulin-dependent protein kinases (DAPK1 and PRKAA2), PKC family (PRKCE, PRKCA, and PRKCG), DNA damage response (DNA-PK and ATM) and stress response related proteins (SGK1). Kinases predicted to be downregulated included electrolyte homeostasis (WNK1), immune response (CAMK4 and PRKCQ) and cytoskeletal rearrangement (EPHA2 and ROCK) related regulators, among others (*row2*; Figure 2G). Similar pathway activation and kinase activity profiles were observed in PBMCs of severe/ICU COVID-19 patients and other *in vitro* models of SARS-CoV-2 infection.[44,64–67] SARS-CoV-2 infection also resulted in activation of other upstream regulators involved in coagulation/wound healing (EDN1 and FN1) and cytokine production (CSF1, CCL2, IRS2, and NCOA3) and suppression of factors involved in antiviral response (PTPRK and PPP2R1A) (Figure 2H). In line with previous reports,[18,22,44,53–55,65] network activity analysis also showed that SARS-CoV-2 infection-mediated activation of translation (EIF2/4), hyperinflammation (IL1B, IL-18) and apoptosis/lymphopenia (CASP3/9) related pathways with concomitant suppression of anti-viral/anti-inflammatory response (NF-kB, IFN type-1, and Jak-STAT) in A549-hACE2 cells (Figures 3A and 3B).

We also evaluated the contribution of RNA/protein abundance to changes at either phosphorylation or secretion level. Consistent with reports of increased cytokine secretion[68,69] and host phosphorylation landscape rearrangement,[65] for nearly all cases of a significantly changed phosphorylation site and/or secreted protein, we did not observe corresponding significant changes in RNA/protein abundance (Figure S3G). These results suggested that, instead of transcriptional regulation, post-translational (i.e., phosphorylation or secretion) regulation is the primary host response to SARS-CoV-2 infection, which would influence protein abundance, at least during the timescale of infection in our study.

G9a inhibition rescues SARS-CoV-2 hijacked pathways

As evidenced by negative overall correlations (RNA-seq = −0.53; proteome = −0.48; phosphoproteome = −0.47; secretome = −0.42), pharmacologic inhibition of G9a led to reversal of SARS-CoV-2-mediated changes in abundance (RNA-seq,

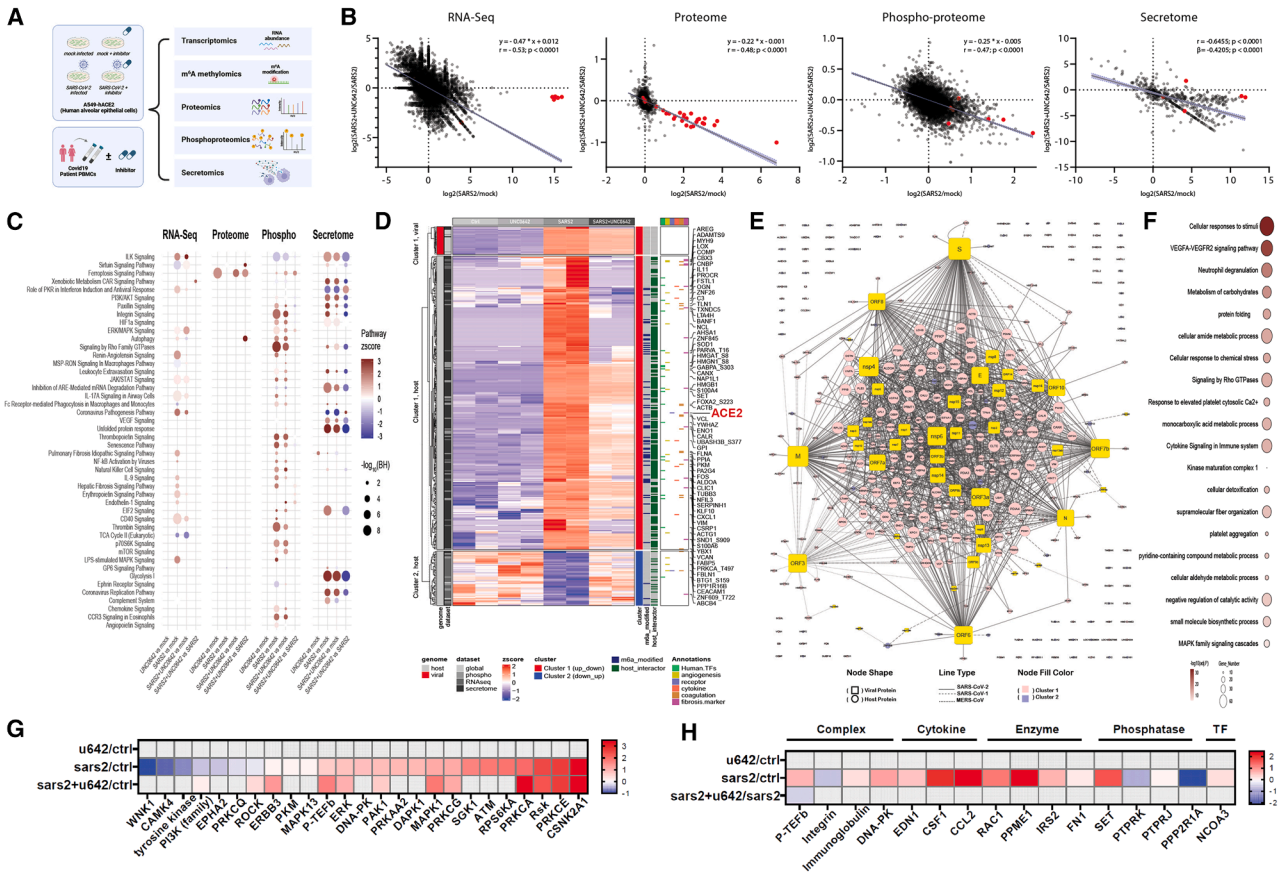

Figure 2. G9a inhibition reverses multi-omic landscape of SARS-CoV-2 infection

(A) Schematic design of multi-omic approaches to dissect G9a regulated pathogenesis of COVID-19 in A549-hACE2 cells and COVID-19 patient-derived PBMCs.

(B) Scatterplots showing that UNC0642 treatment reverses SARS-CoV-2 induced changes to host (black) and viral (red) entities at each omics level in virus-infected A549-hACE2 cells. Linear regression (with 95% CI), slope of regression line (β), and Pearson correlation (r) are overlaid.

(C) Plot summarizing pathway activation z-scores calculated by ingenuity pathway analysis (IPA) based on entities that are differentially regulated at indicated omics levels following SARS-CoV-2 infection and/or UNC0642 treatment of A549-hACE2 cells. Each column corresponds to indicate pairwise comparison. Red represents pathway activation, and blue represents pathway inhibition. The dot size corresponds to adjusted p values.

(D) Heatmap of SARS-CoV-2 dysregulated transcripts (52), proteins (23), phospho-sites (140), and secreted (237) proteins in A549-hACE2 cells whose levels are reversed by UNC0642 treatment. Viral and host entities are clustered separately and further subdivided into two groups, i.e., cluster-1 = upregulated following infection and downregulated upon UNC0642 treatment; cluster-2 = downregulated upon infection and upregulated upon UNC0642 treatment. Annotations on right highlight G9a-regulated m^{6}A-modified transcripts and host interactors of SARS-CoV-1/2- and MERS-CoV-encoded proteins. Six functional clusters include viral receptors and proteases, transcription factors, cytokines/chemokines, coagulation system-related proteins, angiogenesis-associated proteins, and fibrosis markers.

(E) Virus-host interactome map showing that nearly all cluster-1 proteins identified in (D) are host interactors of SARS-CoV-2 (solid line), SARS-CoV-1- (dashed line), or MERS-CoV- (dotted line) encoded proteins. Viral proteins are depicted by yellow rectangles, and host interactors are represented by circles. Size of each node represents connectivity, and node fill color (cluster-1 in pink; cluster-2 in blue) represents coronavirus-dysregulated/inhibitor-reversed proteins.

(F) Gene ontology enrichment analysis for proteins shown in (D and E). All terms with significant over-representation (adjusted $p < 0.05$) are kept, and redundant terms are removed. Dot size represents the number of dysregulated genes/proteins belonging to said term.

(G) Kinase activity scores (-log10(P) < 0.05) calculated by ingenuity pathway analysis (IPA) based on differentially regulated phospho-sites identified in A549-hACE2 cells following SARS-CoV-2/mock infection with or without UNC0642 treatment. Rows represent indicated pairwise comparison, and columns correspond to individual kinase/family (red for activation, blue for deactivation).

(H) Upstream regulator activity (-log10(P) $\leq$ 0.05; activation-score $\geq$ |0.5|) calculated by ingenuity pathway analysis (IPA) using differentially regulated phospho-sites identified in A549-hACE2 cells following SARS-CoV-2/mock infection with or without UNC0642 treatment. Rows represent indicated pairwise comparison, and columns correspond to individual regulator/family (red for activation, blue for deactivation). (See also Figures S3 and S4; Table S2).

proteome), secretion (secretome), and phosphorylation (phosphoproteome) of various viral/host transcripts and proteins in A549-hACE2 cells (Figure 2B). We observed similar reversal in the activity of SARS-CoV-2 dysregulated pathways following G9a inhibition, an effect that was absent in UNC0642-treated mock-infected controls, thereby further associating G9a activity with viral replication and the SARS-CoV-2 dysregulated host response (Figure 2C). Specifically, abundance, secretion, and/or phosphorylation patterns of 351 host or viral entities dysregulated following SARS-CoV-2 were reversed upon UNC0642 treatment.

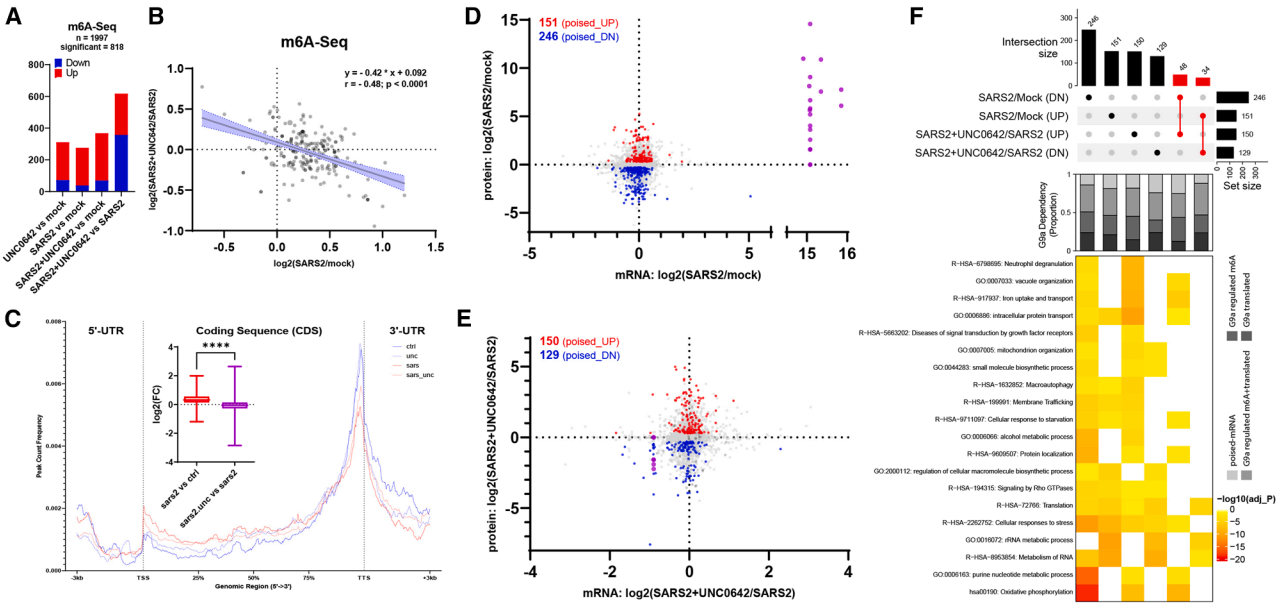

Figure 3. G9a and SARS-CoV-2 co-upregulate m^{6}A modification of select mRNAs involved in proviral host response

(A and B) (A) Number of transcripts with significant difference in m^{6}A modification level, detected using m^{6}A-Seq, following SARS-CoV-2 infection and/or UNC0642 treatment of A549-hACE2 cells (B) UNC0642 treatment reverses SARS-CoV-2-mediated changes in the host m^{6}A methylome. Linear regression line (with 95% CI highlighted), slope of regression line (β) and Pearson correlation (r) are shown.

(C) Distribution of the enriched m^{6}A peaks, respectively, in control (blue line), UNC0642 treated (dotted blue line), SARS-CoV-2 infected (red line), and SARS-CoV-2 infected + UNC0642 treated (dotted red line) A549-hACE2 cells analyzed along the RNA segments. Each transcript was length normalized and ±3 kb from TSS/TTS are included. Boxplot shows an increase in m^{6}A level following SARS-CoV-2 infection (red), compared with uninfected control, which is reversed upon UNC0642 treatment (magenta). Mann-Whitney test was used for statistical analysis (****$p < 0.0001$).

(D and E) Scatterplots depicting transcriptomic and proteomic changes following SARS-CoV-2 infection (D) and UNC0642 treatment (E) of infected A549-hACE2 cells compared to respective controls. Poised mRNAs with statistically significant increases (red) or decreases (blue) in protein expression are highlighted. Number of poised mRNAs (i.e., genes showing differential protein expression without detectable change at the transcript level) is shown (top left). SARS-CoV-2 encoded genes/proteins (showing increases upon SARS2 infection and decreases upon UNC0642 treatment) are highlighted by purple dots.

(F) On top is upset plot showing number and overlap among poised mRNAs identified in (D) and (E). Poised mRNAs dysregulated following SARS-CoV-2 infection whose expression was reversed following UNC0642 treatment are highlighted in red. Stacked bar plot in the middle shows proportion of identified poised mRNAs whose m^{6}A-modification, translation, or both m^{6}A-modification and translation is regulated by G9a/UNC0642. Pathway enrichment for indicated gene sets is shown at bottom. p values were calculated based on the cumulative hypergeometric distribution followed by Benjamini-Hochberg procedure to account for multiple testing. (See also Figures S4 and S5; Table S3).

Most of these entities showing SARS-CoV-2-induced, UNC0642-reversed patterns in "cluster-1" were related to coronavirus pathogenesis, including viral transcripts and proteins, host receptors for virus entry (notably, ACE2), fibrosis markers, cytokines, and coagulation or angiogenesis-related proteins (Figure 2D). Nearly all members of cluster-1 were host interactors of various SARS-CoV-1/2- and MERS-CoV-encoded proteins, further highlighting G9a's function in promoting expression/phosphorylation of host factors necessary for SARS-CoV-2 infection/replication (Figure 2E). Overall, these SARS-CoV-2 promoted, UNC0642-reversed, host-interactors were involved in complexes or pathways related to immune response (e.g., antiviral/stress response, neutrophil degranulation, and cytokine signaling), coagulation or angiogenesis (e.g., platelet aggregation, VEGF signaling), translation (e.g., ribosome biogenesis), energy metabolism (e.g., carbohydrate, carbon, small molecule synthesis), and cell cycle (Figures 2F and S3H).

In parallel, we evaluated the effect of G9a inhibition by UNC0642 on the host response of mock-infected A549-hACE2 cells. Although UNC0642 treatment altered expression, secretion and/or phosphorylation of certain host proteins (Figure S3D), overall, there was negligible effect on the global and phosphoproteomic landscape. Thus, G9a had little effect on host phosphorylation-dependent signaling under noninfected circumstances (i.e., row 1 in Figure 2G). More importantly, in line with global reversal of SARS-CoV-2-mediated changes in abundance and phosphorylation of host and viral proteins, UNC0642 treatment reduced or reversed the kinase activity profile of SARS2 infection (row 3 in Figure 2G). Coincidently, therapeutic targeting of several G9a-regulated kinases that we identified inhibited SARS-CoV-2 infection and replication *in vitro*.[44,64–66] These kinases are functionally associated with growth factor signaling (e.g., MAPK, PI3K/Akt, and TGF-b), protein translation (e.g., mTOR, p38/MAPK), cell cycle (e.g., CDKs), and cytoskeletal rearrangement (e.g., CSNK2A1/2). Similarly, G9a inhibition did not affect the activities of regulators related to coagulation/wound healing, cytokine production, and antiviral response in mock-infected cells but, in contrast, led to stark reversal in activation of these regulators in SARS-CoV-2-infected A549-hACE cells (Figure 2H). Network activity analysis also showed that G9a inhibition reduces activation of pathways

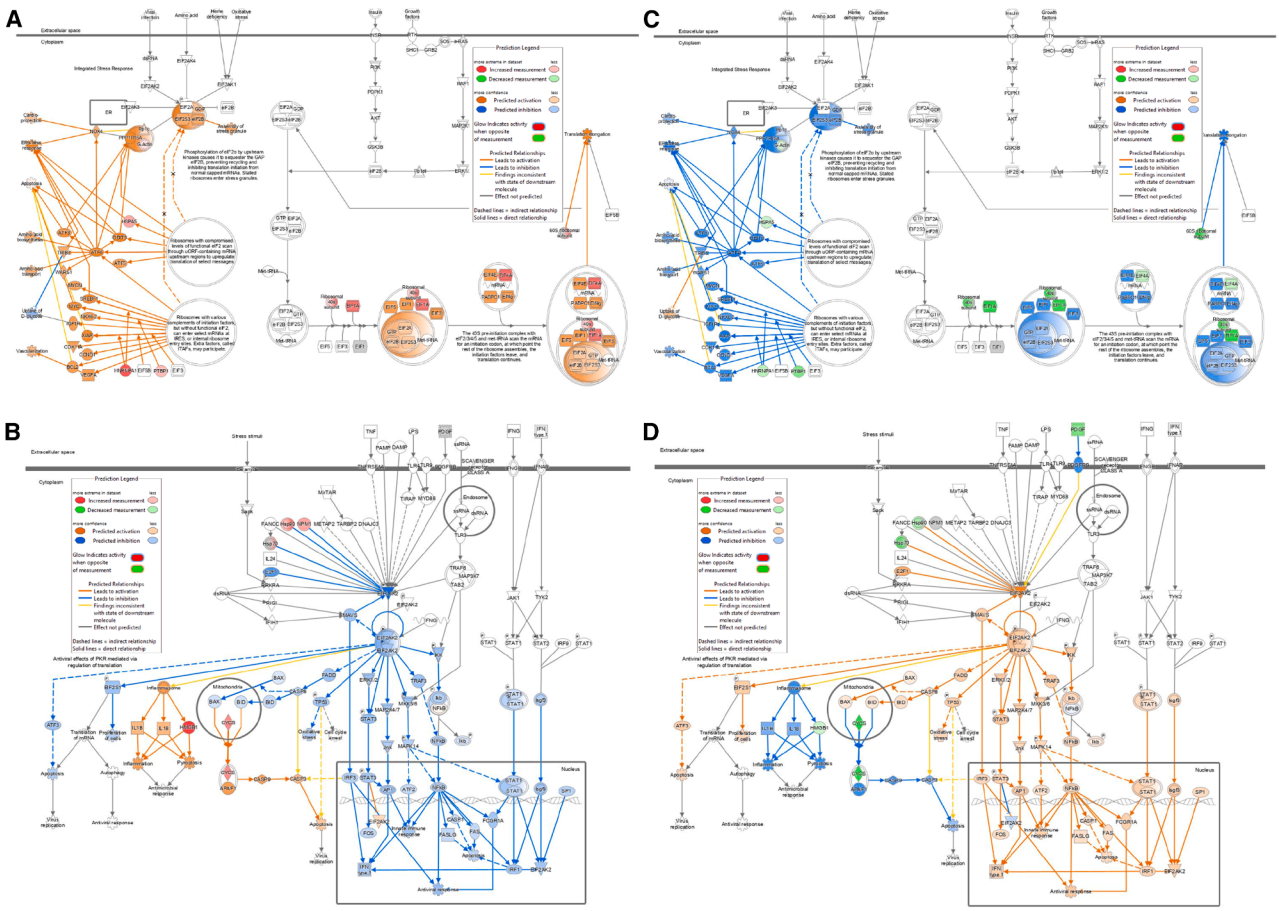

Figure 4. G9a inhibition reversed SARS-CoV-2 dysregulated host pathways related to translation and antiviral response

(A and B) Networks overlaid with gene expression changes following SARS-CoV-2 infection, compared to mock infected controls (i.e., SARS2 vs. Ctrl), show activation of pathways related to translation (EIF2/4), hyperinflammation (IL1B, IL-18), and apoptosis/lymphopenia (CASP3/9) along with concomitant suppression of anti-viral/anti-inflammatory response (NF-kB, IFN type-1, and Jak-STAT) in A549-hACE2 cells. By comparison, (C and D) UNC0642 treatment of SARS-CoV-2 infected cells (i.e., SARS2+UNC0642 vs. SARS2) reversed these changes. Ingenuity pathway analysis was used to generate these networks overlaid with gene expression levels (RNA-seq). Nodes colored red/green represent increased/decreased expression in our dataset, whereas orange/blue colored nodes and edges represent predicted activation/deactivation of said regulators based on our data. Yellow color refers to our identifications that are different from the literature, whereas gray color indicates unpredictable pathway activities. (See also Figure S3; Table S2).

related to translation (e.g., EIF2/4), hyperinflammation (e.g., IL1B, IL-18), and apoptosis/lymphopenia (e.g., CASP3/9) in SARS-CoV-2 infected cells while activating pathways related to anti-viral/anti-inflammatory response (e.g., NF-kB, IFN type-1, and Jak-STAT) (Figure 4). On a pathway scale, these data explain G9a's function in mediating SARS-CoV-2 rewiring of host signaling to promote viral replication and dysregulated immunity.

Yaron et al. implicated phosphorylation of SARS-CoV-2 proteins in viral replication and pathogenesis.[70] Correspondingly, we identified six phosphorylation sites on SARS-CoV-2 encoded proteins, including Orf9b (Ser50), M (Ser213), and N (Ser78, Ser176, Ser412, and Ser413) (Figure 2B; Table S2C). These sites are conserved among coronaviruses, indicative of functional constraint. Top kinase families predicted to phosphorylate these sites include casein kinase II (CK2), glycogen synthase kinase (GSK-3), ribosomal s6 kinase (RSK), and protein kinase C (PKC), suggesting that these kinases may contribute to regulation of viral replication.[65,70,71] This idea is in line with top upstream kinases predicted by our dataset to be induced by UNC0642 to reverse the phospho-proteomic landscape of SARS2 infection. More importantly, UNC0642 treatment of SARS2-infected cells resulted in marked decrease in phosphorylation at four viral sites, including ones on N (Ser78, Ser176, and Ser412) and Orf9b (Ser50), compared to SARS2 infected cells alone (Figure 2B). Mechanistic details and potential functionality of these G9a regulated sites are unknown and warrant further investigation.

In sum, our multiomics correlation analysis revealed that UNC0642 treatment, which had minimal effect in noninfected cells, broadly rescued the widespread SARS-CoV-2-hijacked signaling pathways. Mechanistically, G9a activity regulates the SARS-CoV-2-mediated activities of translation-regulatory kinases such as RSK, supporting the translation-regulatory function of G9a in SARS-CoV-2 replication and the dysregulated host response.

G9a promotes SARS-CoV-2/m^{6}A-coregulated translation for COVID-19 pathogenesis

METTL3 (m^{6}A writer) stabilizes mRNA transcripts by introducing m^{6}A to promote translation.[72,73] In addition, SARS-CoV-2 infection increases expression of m^{6}A regulators, including METTL3, and induces COVID-19 characteristic m^{6}A landscapes in both virus and the host cells or patients, wherein the m^{6}A modification was implicated in viral replication and dysregulation of host immune response.[35–42,46,74,75] Similarly, we showed that, in ET macrophages, G9a and METTL3 co-upregulated translation of certain m^{6}A-modified mRNAs associated with sepsis and ARDS. Depletion of G9a or METTL3 restored T cell function and reduced macrophage activation syndrome.[23] Further, in line with reports of increased expression of RBM15 and WTAP in COVID-19 patient PBMCs, [36] we observed increased expression of METTL3 complex components (RBM15, WTAP) and m^{6}A readers (TRA2A) upon SARS-CoV-2 infection, which was suppressed by UNC0642 treatment in SARS-CoV-2 infected cells (Figure S3I). In correlation with UNC0642-suppressed SARS-CoV-2 replication (Figures 1E and 2B), our results highlighted a triggering possibility that G9a is the upstream regulator of SARS-CoV-2 hijacked, m^{6}A-mediated translation of proteins associated with COVID-19 pathogenesis. Thus, targeting G9a represents both a virus- and a host-directed mechanism of COVID-19 therapeutic action.

To investigate exactly how active G9a assists SARS-CoV-2 to hijack the host translation pathways, we characterized the function of the ChaC-identified interaction between G9a and METTL3 in SARS-CoV-2 induced pathogenesis. Specifically, we examined whether and how G9a activity would influence the distribution of m^{6}A on cellular transcripts during infection. Accordingly, using MeRIP-Seq, we identified m^{6}A-modified transcripts that had SARS-CoV-2 induced changes and which were reversed by UNC0642 treatment in infected A549-hACE2 cells. Like other omics datasets, we observed a clear principal component separation between mock and infected cells, and UNC0642 treatment resulted in distinct host m^{6}A landscape (Figure S4A). Nearly two thousand m^{6}A-modified transcripts were identified with 818 transcripts having differential m^{6}A abundance following infection and/or UNC0642 treatment (Figure 3A; Table S3A). Coincident with elevated m^{6}A regulator expression in A549-hACE2 cells following SARS-CoV-2 infection (Figure S3I), and previous reports for A549-hACE2 cells and COVID-19 patient PBMCs,[42,45,46] we detected an overall increase in m^{6}A abundance following infection, compared with uninfected controls; this effect was reversed upon UNC0642 treatment as evidenced by the overall negative correlation of −0.48 (Figures 3B and 3C). Specifically, SARS-CoV-2 infection led to increased m^{6}A modification in the 5′-UTR and coding sequence (CDS) regions along with a concomitant decrease in m^{6}A abundance around the 3′-UTR of host transcripts. However, UNC0642 treatment reversed these SARS-CoV-2-mediated changes in CDS m^{6}A levels (decrease) and 3′-UTR (increase) regions, and led to decreased m^{6}A in the 5′-UTR regions in general (Figure 3C). Most SARS-CoV-2 dysregulated, UNC0642-reversed, m^{6}A-modified transcripts were involved in pathways related to type I/II interferon regulated genes involved in immunity (viral infection, neutrophil degranulation), cell cycle (mitosis, G2/M transition), translation, RNA splicing/processing, cytoskeletal rearrangement, and energy metabolism (carbohydrates, glucose, glycolysis, and steroids) (Figures S4B and S4C). Interestingly, most transcripts with differential m^{6}A did not exhibit corresponding changes in mRNA expression (Figure S4D); thus, increased m^{6}A following SARS-CoV-2 infection was not due to changes at the transcriptional level but, instead, due to a post-transcriptional host response to virus infection.

G9a directs translation of viral and host proteins for SARS-CoV-2 replication and dysregulated host response

Following virus entry into host cells, viral mRNAs are "poised" to rapidly undergo translation and produce virus replication proteins and trigger translation of specific mRNAs for the host response. However, little is known about how these poised mRNAs are regulated during SARS-CoV-2 pathogenesis. To further elucidate the mechanism of G9a-mediated translation in SARS-CoV-2 replication and associated pathogenesis, we compared transcriptomic (RNA-seq) and LFQ proteomic datasets from the A549-hACE2 cells with versus without SARS-CoV-2 infection or with and without G9a inhibitor treatment. These multi-omics comparisons identified G9a-regulated, poised mRNAs, i.e., genes that showed changes in protein expression without any significant change in corresponding mRNA levels following SARS-CoV-2 infection. As expected, we detected 397 (151 upregulated; 246 downregulated) and 279 (150 upregulated; 129 downregulated) differentially expressed poised mRNAs following SARS-CoV-2 infection with versus without UNC0642 treatment (Figures 3D and 3E; Table S3B). SARS-CoV-2 infection reshaped host signaling to produce more protein from viral infection, translation/rRNA-biogenesis and cell cycle-related mRNAs, whereas infection reduced translation of host immunity, stress response, and energy metabolism-related genes (Figure 3F; columns 1 to 4). More importantly, these SARS-2 mediated changes in expression of host poised mRNAs were largely mitigated (120 total; 48 down/up; 34 up/down) following UNC0642 treatment of infected cells (Figure 3F; columns 5–6). Lastly, the majority of SARS-CoV-2 regulated poised mRNAs whose expression was reversed by UNC0642 were also identified as "G9a-translated" proteins that carried G9a/METTL3-coregulated m^{6}A modification in ET macrophages (Figure 3F). These results underpinned the crucial activity of G9a in SARS-CoV-2 mediated hijacking of host translational machinery to increase virus production and evade host cell immune responses. Together, we showed that G9a upregulated m^{6}A of select host mRNAs following SARS-CoV-2 infection to promote translation of transcripts functionally related to immune response, rRNA/ribosome, and viral entry/egress.

SARS-CoV-2-induced, G9a-mediated translation contributes to COVID-19 complications

To ascertain the clinicopathologic relevance of the G9a translational mechanism of COVID-19 pathogenesis, we conducted transcriptomic (RNA-seq), epi-transcriptomic (m^{6}A/RIP-seq), and LFQ proteomic experiments to identify G9a-regulated, poised mRNAs from *ex vivo* culture of COVID-19 patient derived PBMCs. Briefly, akin to the results from A549-hACE2 cells, we

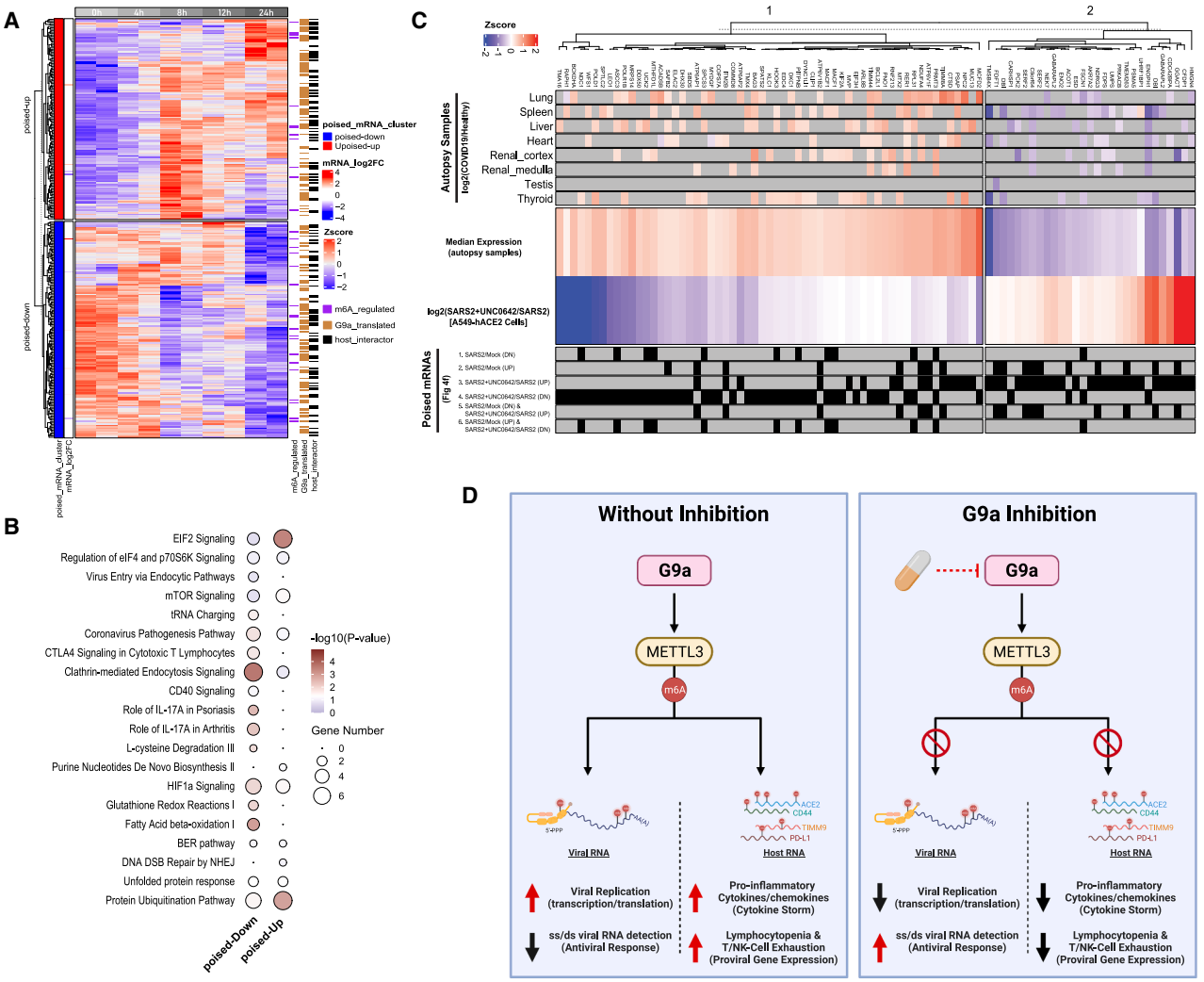

Figure 5. G9a regulates poised mRNA expression in COVID-19 patient PBMCs and autopsy samples

(A) Heatmap summarizing transcriptomic (RNA-seq), epi-transcriptomic (meRIP-seq), and proteomic (LFQ-MS) effects of UNC0642 inhibition in COVID-19 patient PBMCs. Briefly, *ex vivo* cultures of patient PBMCs were treated with 1 μM UNC0642/DMSO and samples collected at indicated time points for LFQ-MS; RNA-seq and meRIP-seq were performed at 24 h. In line with A549-hACE2 results, most UNC0642 regulated genes showed differential protein expression without detectable change at transcript level (i.e., poised mRNAs). Annotations on right show that most of these genes are translated in a G9a-dependent manner in ET macrophages, with a subset carrying G9a regulated m^{6}A modification, and are host interactors of SARS-CoV-1/2- and MERS-CoV-encoded proteins.

(B) Pathway enrichment analysis for G9a regulated poised mRNAs shown in (A). All terms with significant over-representation (adjusted $p < 0.05$) are kept, and redundant terms are removed. Dot size corresponds to the number of dysregulated genes/proteins in said term.

(C) Heatmap showing that several proteins with multi-organ dysregulation in autopsy samples from COVID-19 patients are, in fact, encoded by SARS-CoV-2/G9a-coregulated poised mRNAs, and their expression was reversed upon UNC0642 treatment of SARS-CoV-2 infected A549-hACE2 cells. Rows 1–8: log2 (COVID-19/healthy) ratio for indicated organs; Rows 9: Median expression of indicated proteins in autopsy samples. Row 10: log2 (SARS2+UNC0642/SARS2) ratio in A549-hACE2. Rows 11–16: indicate whether said protein is encoded by poised mRNAs identified in earlier (Figure 3F) comparisons.

(D) Possible mechanisms of G9a action. Briefly, SARS-CoV-2 infection uses G9a-METTL3-m6A axis to promote m^{6}A modification on (1) host transcripts to promote expression of lymphopenia, T/NK cell exhaustion and hyperinflammation related proteins, and (2) SARS-CoV-2 genome to promote viral transcription/translation and evade RIG-1 dependent sensing and activation of innate immune response and ensuing IFN-β/type-I IFN antiviral response. We show that G9a inhibition reverses SARS-CoV-2 mediated rewiring of m^{6}A epi-transcriptome to hinder SARS-CoV-2 replication, suppress expression of pro-inflammatory cytokines, and reduce expression of markers associated with T/NK cell exhaustion, including PD-L1 and other proteins involved in lymphopenia. Created in BioRender. M, A. (2025) https://BioRender.com/akfy5mv (See also Figure S5; Table S4).

identified 292 differentially expressed proteins that were coded by poised mRNAs, most without a corresponding change in transcript level, following UNC0642 treatment of patient PBMCs (Figure 5A; Table S4A). Several proteins were host interactors of various SARS-CoV1/2- and MERS-CoV-encoded proteins and, partially by m^{6}A modification of transcripts, their turnover/translation was regulated in a G9a-dependent manner in ET macrophages (Figure 5A). Overall, G9a regulates protein

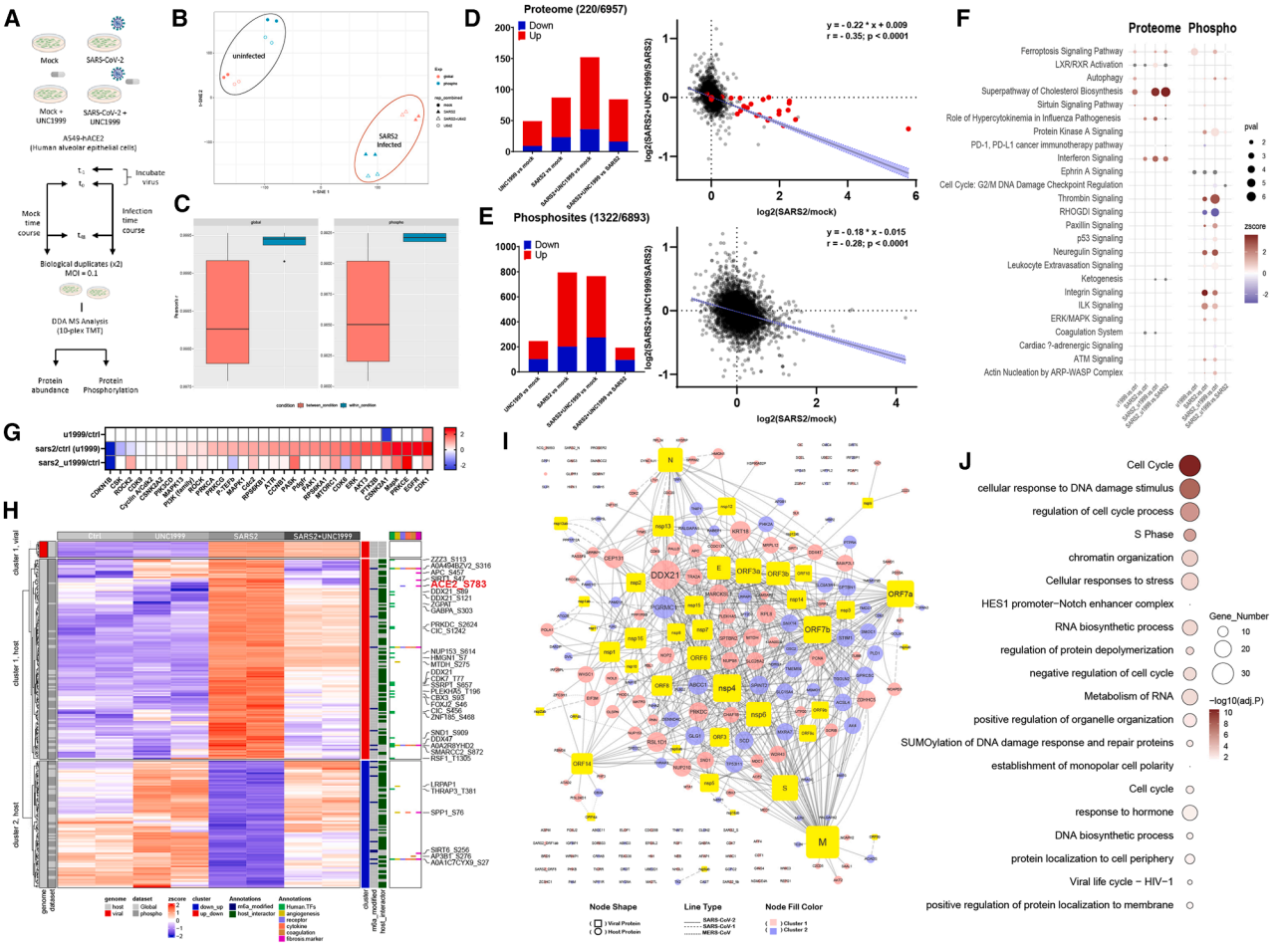

Figure 6. Ezh2 inhibition reverses proteomic landscape of SARS-CoV-2 infection

(A) Schematic overview of SARS-CoV-2 infection and Ezh2 inhibitor treatment of A549-hACE2 cells. Briefly, cells were infected with SARS-CoV-2 (MOI = 0.1). After 1 h of virus uptake, media were switched, and cells harvested 48 hpi with/without UNC1999 treatment. Proteins were digested and 10-plex TMT-labeled followed by DDA-based MS to detect global changes in protein abundance and phosphorylation. All experiments were performed in biological duplicate.

(B) The t-distributed stochastic neighbor embedding (t-SNE) visualization of significantly dysregulated proteins in tested conditions (shape) and datasets (color).

(C) Correlation between replicates within a biological condition (red) and across biological conditions (green). Boxplots depict median (horizonal lines), inter-quartile range (boxes), maximum and minimum values (vertical lines), and outliers (solid circles).

(D) Bar plots depicting number of dysregulated proteins (red = up; blue = down) for indicated comparisons in UNC1999-treated proteomic dataset from A549-hACE2 cells. Total number of identified (n) and dysregulated (significant) entities is mentioned on top. Scatterplot on right shows that UNC1999 treatment reverses SARS-CoV-2 infection mediated changes to host (black) and viral (red) proteins in A549-hACE2 cells. Linear regression (with 95% CI), slope of regression line (β) and Pearson correlation (r) are overlaid.

(E) Bar plot shows number of dysregulated phospho-sites (red = up; blue = down) for indicated comparisons in A549-hACE2 cells. Total number of identified (n) and dysregulated (significant) entities is mentioned on top. The scatterplot on right shows that UNC1999 treatment reverses SARS-CoV-2 infection-mediated changes host phospho-proteome. Linear regression (with 95% CI), slope of regression line (β) and Pearson correlation (r) are overlaid.

(F) Plot summarizing pathway activation scores estimated using differentially regulated entities in global/phospho-proteomic datasets following SARS-CoV-2 infection and/or UNC1999 treatment of A549-hACE2 cells. Each column corresponds to indicated pairwise comparison. Red represents pathway activation, and blue represents pathway inhibition. The dot size corresponds to adjusted p values. Redundant terms were removed.

(G) Kinase activity scores (-log10(P) < 0.05) calculated by ingenuity pathway analysis (IPA) using based on differentially regulated phospho-sites identified in A549-hACE2 cells following SARS-CoV-2/mock infection with or without UNC1999 treatment. Rows represent indicated pairwise comparison, and columns correspond to individual kinase/family (red = activation, blue = deactivation).

(H) Heatmap of SARS-CoV-2 dysregulated, UNC1999 reversed, proteins/phospho-sites in A549-hACE2 cells. Viral and host entities are clustered separately and further subdivided into two groups (cluster1 = up following infection and down upon UNC1999 treatment; cluster2 = down upon infection and up upon UNC1999 treatment). Annotations on right highlight m^6A-modified transcripts (identified by MeRIP-Seq) and host interactors of SARS-CoV-1/2- and MERS-CoV-encoded proteins. Lastly, six functional clusters of viral receptors and proteases, transcription factors, cytokines/chemokines, coagulation system-related proteins, angiogenesis-associated proteins, and fibrosis markers are included with their names highlighted.

(legend continued on next page)

expression/abundance of transcripts related to translation, immunity/infection, lipid metabolism, DDR, cellular energetics, ubiquitination, and unfolded protein response in patient PBMCs (Figure 5B). Like A549-hACE2 cells, UNC0642 treatment of COVID-19 patient PBMCs also reversed SARS-CoV-2 regulated m^{6}A modification in the CDS (decrease) and 3′-UTR (increase) regions of host transcripts. However, unlike A549-hACE2 cells, overall m^{6}A (particularly in the promotor/5′-UTR region) increased following UNC0642 treatment (Figure S5A), possibly owing to cell-typic differences in m^{6}A regulator expression. Overall, most m^{6}A modified transcripts in control (DMSO) patient PBMCs belonged to type I/II interferon regulated genes (Figure S5B) involved in adaptive immune response pathways, translation, infection/endocytosis, blood coagulation, and antibiotic response, a pattern largely absent from UNC0642-treated patient PBMCs (Figure S5C).

Notably, several of the virus/G9a-dysregulated and inhibitor-reversed entities identified earlier (Figure 2D) are known markers of Long COVID or post-acute sequelae of SARS-CoV-2 infection,[76] blood/plasma markers of severe COVID-19,[77,78] and are dysregulated in autopsy samples[76] (Figure S5E). Thus, from our A549-hACE2 global proteomics (LFQ+TMT) datasets, we assessed clinical data[31] to identify 88 SARS-dysregulated/G9a-reversed proteins that showed similar aberrant expression in multi-organ proteomics data from autopsy samples (Figure 3C), with nearly all transcripts carrying G9a regulated m^{6}A modification in ET macrophages, A549-hACE2 cells, and/or COVID-19 patient PBMCs (Table S4B). As expected, these G9a regulated patient-specific proteins were involved in immunity (neutrophil degranulation/VEGF signaling/stress response), energy metabolism, and cellular transport/localization pathways (Figure S5D). Taken together, we show that G9a regulates translation of certain poised mRNAs in COVID-19 patient PBMCs and autopsy samples following SARS-CoV-2 infection, at least partly by the m^{6}A modification pathway, further establishing the clinicopathological relevance of our multi-omics results. More significantly, these COVID-19 proteomic and phosphoproteomic landscapes can be reversed by inhibitor treatment, indicating possible clinical efficacy of G9a inhibitors for COVID-19 therapy or treatment of COVID-19 sequalae.

Pharmacological intervention of G9a-associating translation machinery suppressed SARS-CoV-2 pathogenesis

Because EZH2 may be a key factor in G9a-mediated translational regulation of COVID-19 pathogenesis, we inhibited EZH2 with UNC1999 and measured proteome and phosphoproteome changes in SARS-CoV-2 infected A549-hACE2 cells. UNC1999 treatment resulted in a distinct proteomic landscape compared with controls (Figures 6A and 6B; Tables S5A and S5B) with good reproducibility between and across replicates (Figure 6C). From a systems view, UNC1999 treatment led to significant reduction in expression of SARS-CoV-2 encoded proteins along with overall reversal in SARS-CoV-2 induced changes in the host proteome (correlation = −0.349; Figure 6D) and phosphoproteome (correlation −0.281; Figure 6E). Notably, similar to effects of G9a inhibition, UNC1999 treatment reversed SARS-CoV-2 induced changes primarily at the phosphoproteomic level as opposed to changes in protein abundance in SARS-CoV-2 infected cells (Figures 6D and 6E). Most of these UNC1999-affected phosphoproteins are functionally associated with coronavirus replication, virus entry/egress, immune response, and cholesterol signaling (Figure 6F). Specifically, on the basis of quantitative phosphoproteomic identification of SARS-CoV-2-induced proteins whose phosphorylation was reversed by UNC1999, we found that SARS-CoV-2 infection activated multiple kinase-mediated signaling pathways, including MAP/ERK pathway (MAPK1, MAPK13, and ERK), RTK family (EGFR and PDGFR), cell cycle (CDK1/6 CCNB1, and CDC2), Casein kinase (CSNK2A1/2), AKT/PI3K pathway (MTORC1, RPS6KA1/B1, and AKT3), Ca^{2+}/calmodulin-dependent protein kinases (DAPK1 and PRKAA2), PKC family (PRKCA, PRKCE, and PRKCG) and DDR (ATM and PLK1) related kinases. In parallel, decreased activity was observed for specific kinases related to cell cycle (CDKN1B) and cytoskeleton regulator (ROCK2) (Figure 6G). Overall, the abundance and/or phosphorylation pattern of 235 entities dysregulated by SARS-CoV-2 infection were reversed upon UNC1999 treatment, including several coronavirus pathogenesis related entities, e.g., viral transcripts/proteins, host receptors (ACE2), fibrosis markers, cytokines, coagulation/angiogenesis-related proteins, and transcription factors (Figure 6H). Most of these proteins were host interactors of SARS-CoV-1/2- MERS-CoV-encoded proteins, further highlighting Ezh2's function in promoting expression and/or phosphorylation of host factors necessary for SARS-CoV-2 infection and replication (Figure 6I). Together, these SARS-CoV2-induced/UNC1999-reversed host interactors were involved in antiviral/stress response, cell cycle, RNA metabolism, protein transport, and DDR related pathways (Figure 6J).

Pharmacological inhibitors of Ezh2 are approved for treatment of epithelioid sarcoma and follicular lymphoma[61]; therefore, these inhibitors could be repurposed for COVID-19 therapy. Thus, we investigated the effect of tazemetostat, an FDA-approved inhibitor of Ezh2, on coronavirus-related proteins in clinical setting, i.e., *ex vivo* culture of PBMCs from two severe COVID-19 patients. Out of 4221 proteins quantified by LFQ-MS, 420 proteins (305 down, 115 up) were differentially regulated following treatment (Figure S6A; Table S5C). Strikingly, 193 dysregulated proteins (157 down, 36 up) were host interactors of SARS-CoV-1/2- and MERS-encoded proteins, clearly demonstrating that these tazemetostat-downregulated proteins are required for efficient SARS-CoV-2 replication or infection. Overall, tazemetostat-dysregulated proteins were involved in viral-entry (i.e., coronavirus pathogenesis, endocytosis, and phagocytosis), translation (EIF2,

(I) Virus-host interactome map showing that most of the proteins identified in (H) are host interactors of SARS-CoV-2 (solid line), SARS-CoV-1- (dashed line) or MERS-CoV- (dotted line) encoded proteins. Viral proteins are depicted by yellow rectangles, and host interactors are represented by circles. Size of each node represents connectivity, and node fill color (cluster1 = pink; cluster2 = blue) represents coronavirus-dysregulated/Ezh2-reversed proteins.
(J) Gene ontology enrichment analysis for proteins shown in (H and I). All terms with significant over-representation (adjusted $p < 0.05$) are kept, and redundant terms are removed. Dot size represents the number of dysregulated proteins belonging to said term. (See also Figure S6; Table S5).

mTOR, eIF4, and p70S6K), immune response (interleukin/cytokine, neutrophil, macrophage, inflammation, NF-kB, apoptosis, and autophagy) and cellular metabolism (nucleotide, cholesterol, and amino acid) related signaling (Figure S6B). Several proteins in these pathways are among the top hits/host factors necessary for coronavirus pathogenesis, characterized by multiple genome-wide siRNA/CRISPR studies.[21,60,79–82] For example, tazemetostat suppressed the expression of 12 host factors known to hinder SARS-CoV-2 infection, including CSTL/VPS34 (spike cleavage and membrane fusion), PIK3C3 (endosome maturation) and ERMP1 (ER/Golgi-trafficking) (Table S5C). Systematic analysis of disease-related signaling cascades showed a strong suppression of viral/bacterial infection and immune system activation (Figure S6C), further corroborated by UNC1999-mediated suppression of translation (EIF2/4) and inflammation (NF-kB, IL-6, and IL-8) related network activity (Figures S6D and S6E). Together, Ezh2 inhibition compromised SARS-CoV-2-mediated changes to host proteome and phosphoproteome, thereby hindering SARS-CoV-2 replication in A549-hACE2 cells and, more importantly, Ezh2 inhibition suppressed (1) host interactors of SARS-CoV-2 encoded proteins, (2) host factors required for efficient SARS-CoV-2 infection/replication, and (3) critical pathways involved in coronavirus pathogenesis in COVID-19 patient PBMCs. Combined results indicated that EZH2 is a key component of the G9a translational regulatory machinery whereby G9a and Ezh2 cooperatively promote SARS-CoV-2 pathogenesis primarily at the translational and/or post-translational level.

DISCUSSION

We investigated how SARS-CoV-2 hijacks the host response mechanism to produce specific proteins that are the primary executers of COVID-19 pathogenesis. In line with the fact that dysregulated translation of specific proteins directly contributes to disease pathogenesis, we established a noncanonical G9a-METTL3/m^{6}A-Ezh2 axis that broadly regulates widespread SARS-CoV-2-hijacked translation pathways[32] associated with viral replication, hyperinflammation, T cell exhaustion, and suppressed host antiviral response (Figure 5D, left panel). In parallel, we revealed the mechanism of inhibitor action for both virus- and host-directed therapeutics of COVID-19, whereby G9a/Ezh2 inhibitors reverse SARS-CoV-2 dysregulated translation processes (Figure 5D, right panel). Importantly, these mechanistic findings are highly correlated with *in vivo* efficacy of G9a inhibitor (UNC0642) in reducing SARS-CoV-2 growth and infection-induced lung damage.[25] Given higher resistance barrier, broader activity against coronavirus strains/species, and potential synergy with other direct-acting antiviral drugs,[83,84] our approach of targeting G9a-regulated mechanisms of COVID-19 pathogenesis represents broad-spectrum, precision therapeutics to counter any emerging coronavirus variant and to prevent COVID-19 sequelae.

Evidently, m^{6}A modification is the most prevalent hallmark of SARS-CoV-2-hijacked translation pathways. Increased viral m^{6}A modification stabilized SARS-CoV-2 transcripts[36] to promote replication and translation of SARS-CoV-2 genome[35–37] and to evade RIG-1-dependent sensing and activation of the innate immune response.[74] Simultaneously, SARS-CoV-2 infection rewired the host m^{6}A epitranscriptome to promote programmed cell death in lymphocytes[35] and upregulate expression of pro-viral and inflammatory response genes.[35,37,46,75] As an m^{6}A writer, METTL3 interacts with SARS-CoV-2 RNA-dependent RNA polymerase (RdRp) in the host to facilitate SARS-CoV-2 RNA m^{6}A modification and viral replication.[37] Similarly, an elevated level of METTL3 and m^{6}A readers, such as RBM15B, IGF2BP1, hnRNPA1, coupled with a decrease in m^{6}A demethylase (FTO, ALKBH5) expression was reported in SARS-CoV-2 infected cell lines[35–38] and clinical isolates from severe COVID-19 patients.[39–42] Correspondingly, we identified by ChaC most of m^{6}A regulators (e.g., writers or readers) as the COVID-19 phenotypic interactors and showed that G9a inhibition reversed the SARS-CoV-2-induced m^{6}A landscape (Figures 3B and 3C); thus, via the METTL3-m^{6}A axis, G9a regulates select SARS-CoV-2-hijacked translation pathways. For example, in correlation with the observation that compromised antigen presentation by METTL3^{hi}CD155^{hi} macrophage cells diminishes antiviral T cell response against SARS-CoV-2 antigens in COVID-19 patients with coronary artery disease,[85] we found that G9a inhibition reversed the level of select m^{6}A mRNAs associated with macrophage proliferation, T cell dysfunction, and dysregulation of blood coagulation. Presently, in the absence of good clinical/pre-clinical molecules that target m^{6}A regulators (METTL3), our results demonstrate that inhibition of G9a, the upstream regulator of SARS-CoV-2 induced m^{6}A epitranscriptome, represents a host mechanism-directed therapeutic approach to combat SARS-CoV-2 infection.

Multiomics-correlated analysis identified poised mRNAs whose translation was triggered by SARS-CoV-2 infection in a G9a activity-dependent manner. As a result, G9a translates these poised mRNAs into proteins that promote SARS-CoV-2 replication, including ACE2 binding/entry and *pathogenesis*. Further, phosphoproteomic data showed that G9a regulated host kinase signaling, indicating that most regulation of SARS-CoV-2 pathogenesis occurs by post-translational modification (phosphorylation or secretion) as opposed to regulating protein abundance.

Pathogenic influenza and β-coronaviruses (SARS-CoV-1/2 and MERS-CoV) suppress transcription of IFN-regulated genes[86–88] by multiple mechanisms that include increased repressive marks (H3K9me and H3K27me) and histone mimicry employed by SARS-CoV-2.[56,57] Interestingly, Hu et al. reported that EZH2 interacts with METTL3[58] and Yi et al. described a PRC2-independent function for EZH2 in IRES-dependent translation,[43] raising the possibility that EZH2 might be a key component of the G9a-associated translational regulatory machinery that promotes COVID-19 pathogenesis. In this study, we showed that multiple members of G9a, EZH2, and METTL3 complexes were upregulated in nasopharyngeal swabs and/or autopsy samples from severe COVID-19 patients (Figures S1A and S1B). G9a and Ezh2 interacted with the same translational regulators in ET macrophage and COVID-19 patient PBMC cells (Figures 1B and 1C) to help G9a promote turnover of host interactors of SARS-CoV-1/2- and MERS-encoded proteins and other pro-viral host factors (Figure 1D). Drugs targeting G9a and Ezh2 were potent inhibitors of SARS-CoV-2 replication (Figure 1E) and reversed multi-omic effects of SARS-CoV-2

infection in A549-hACE2 cells and COVID-19 patient PBMCs (Figures 2, 3, 4, 5, and 6; S3–S6). We identified a mechanistic axis by which G9a remodels viral and host m^{6}A epi-transcriptome following SARS-CoV-2 infection (Figures 3 and 5) to promote viral replication and infection by upregulating expression of various viral receptors (including ACE2), transcription factors, cytokines (and their receptors), coagulation/angiogenesis related proteins, and fibrosis markers in A549-hACE2 and COVID-19 patient PBMCs (Figure 2) with said proteins showing similar dysregulation pattern in multiorgan autopsy samples taken from deceased COVID-19 patients (Figure 5). Together, we showed that G9a inhibition suppressed SARS-CoV-2 replication while reducing inflammatory cytokine and proviral gene expression to enhance antiviral response (Figure 5D). Overall, we extend G9a function(s) beyond transcription to translational regulation during COVID-19 pathogenesis.

Our inhibitor proteomics data provided the mechanistic details about *in vivo* efficacy of inhibitor treatment of COVID-19. In correlation with inhibition of SARS-CoV-2 replication, inflammation, and lung fibrosis by UNC0642 in a hamster infection model,[25] we identified in SARS-CoV-2 infected A549-hACE2 cells numerous proteins showing SARS-CoV-2-induced, UNC0642-reversed/reduced expression (e.g., ADAMTS9, AREG, FOS, IL11, and LOX), secretion (e.g., ACE2, AHSA1, CALR, COMP, FABP5, HMGB1, SERPINH1, SOD1, TXNDC5, and VIM) and/or phosphorylation. These G9a-translated proteins include SARS-CoV-2 receptors (ACE2 and CEACAM1), fibrosis markers, inflammatory cytokines, and angiogenesis/coagulation factors, whose functions are associated with virus replication, inflammation, and lung fibrosis (Figures 2D and 6H; Tables S2 and S5). In addition, corresponding to the *in vivo* effect of DZNep, an S-adenosylhomocysteine hydrolase inhibitor of Ezh2 that reduces SARS-CoV-2 load and virus-induced inflammation in C57BL/6 mice,[89] Ezh2 inhibition by UNC1999 treatment affected similar G9a-translated pathologic pathways (Figure 6H; Table S5). These animal-to-human conserved effects confirmed the *in vivo* or clinicopathologic accuracy of G9a translation regulatory mechanisms of COVID-19 pathogenesis and the G9a-target mechanism of COVID-19 therapeutics. Interestingly, AMPK-mediated phosphorylation of EZH2 at T311 is known to suppress the activity of the PRC2 complex.[90] Recently, we developed a USP7-based deubiquitinase-targeting chimera (DUBTAC) that stabilizes AMPK.[91] It would be interesting to investigate whether this DUBTAC targeting AMPK also hinders SARS-CoV-2 replication through the EZH2/G9a-driven translation mechanism reported here.

Emerging and future coronaviruses require new therapeutics to increase antiviral breadth, combat emerging resistance and improve tolerability. Drugs that target G9a and its interacting protein EZH2 have known safety profiles and targeting methyltransferase complexes in a transient manner offers several advantages in the regulation of sarbecovirus infection. First, the translation regulatory function of G9a, by way of the G9a-METTL3-m^{6}A axis, is anticipated to be synergistic with existing direct-acting antiviral (remdesivir, molnupiravir, and paxlovid) and host immunomodulatory drugs (dexamethasone). Second, by suppressing secretion of ACE2 (Figure 2D), G9a inhibitors can hinder entry of ACE2-dependent viruses including SARS-CoV-1/2, HCoV-NL63, and various bat sarbecoviruses with potential for spillover to humans.[92–94] Third, G9a targets multiple stages of the SARS-CoV-2 replication/life cycle, exhibiting multifaceted effects that include reduction in infection-induced hyperinflammation and thrombosis/lung-fibrosis marker expression, curbing T cell depletion/dysfunction and suppression of viral replication (Figures 1D and 5D; also see ref; [30]). Fourth, the m^{6}a modification pathway is hijacked by several RNA viruses (e.g., influenza A, HCV, HBV, EV71, and HIV) for propagation and persistence[95–98] and, accordingly, sites of m^{6}A modification are conserved in various SARS-CoV-2 variants,[45] highlighting a potential evolutionary function of these sites in transmission and epidemiology. Indeed, Batista-Roche et al. reported that SARS-CoV-2 variants (epsilon > B.1.1.519 > alpha/gamma > omicron) and vaccination status (unvaccinated > partially vaccinated > vaccinated) modulated genome and/or viral m^{6}A levels differentially.[99] Taken together, our data suggest that methyltransferase inhibitors (G9a/Ezh2) can be repurposed into broad-spectrum antivirals and represent a novel class of host mechanism-directed therapeutics to counter emerging drug resistance and infection.

Limitations of the study

Findings in this study should be considered in light of the following limitations, most of which require additional research. First, a comprehensive investigation that discriminates between the canonical (transcriptional repression) and noncanonical (translation promotion) functions of the G9a complex during viral infection is needed. Second, the exact function of EZH2 during SARS-CoV-2 infection requires further investigation. Third, comprehensive studies are needed in animal and/or human models (1) to further understand mechanistic details, (2) to evaluate efficacy and synergy of G9a/Ezh2 inhibition in combination with existing direct-action and immunomodulatory antivirals, and (3) to study potential antiviral activity against other m^{6}A modification dependent RNA viruses (e.g., influenza A, HCV, HBV, EV71, and HIV). Third, the influence (or association) of gender on the results of this study has not been investigated. Lastly, COVID-19 accelerates Alzheimer's-related symptoms and dementia,[100,101] and we recently reported on development of a blood-brain-barrier penetrant G9a inhibitor that reversed m6A modification and expression of AD-dysregulated transcripts to reverse cognitive and noncognitive effects of Alzheimer's in multiple mouse models.[47] Thus, it will be interesting to study the effects of G9a inhibition in mouse models of Alzheimer's with COVID-19.

RESOURCE AVAILABILITY

Lead contact

Requests for further information and resources should be directed to and will be fulfilled by the lead contact, Xian Chen (xianc@email.unc.edu).

Materials availability

This study did not generate new unique reagents.

Data and code availability

- RNA-seq and MeRIP-seq datasets have been deposited to the GEO repository (GSE282914) and are publicly available as of the date of

publication. Mass spectrometry proteomics datasets have been deposited to the ProteomeXchange Consortium via the PRIDE partner repository (PXD058743) and are publicly available as of the date of publication.

- This paper does not report original code.
- Any additional information required to reanalyze the data reported in this paper is available from the lead contact upon request.

ACKNOWLEDGMENTS

This work was supported in part by grants NIH R21AG071229, 1R41AG085859-01, 1R41DK133051-01A1, R01 GM133107-01, and UNC University Cancer Research Fund (to X.C.). P.-Y.S. was partially supported by awards from the Sealy & Smith Foundation, the Kleberg Foundation, the John S. Dunn Foundation, the Amon G. Carter Foundation, the Summerfield Robert Foundation, and the Edith and Robert Zinn Foundation. NIH R35NS116843 (to H.S.), R01HD088626, R01AG084184, and an endowed professorship from the Icahn School of Medicine at Mount Sinai (to J.J.). NIH R01 NS125778 and John S. Dunn Research Foundation (to P.W.). NIH R35NS097370 and Dr. Miriam and Sheldon G. Adelson Medical Research Foundation (to G.-L.M.). MS1262 is protected by US provisional patent applications jointly filed by Mount Sinai and UNC-CH.

AUTHOR CONTRIBUTIONS

X.C. conceived, designed, supervised the project, and wrote the manuscript. A.M. analyzed and interpreted data and wrote the manuscript. L.X. performed inhibitor treatment, sample preparation and processing for MS/MS experimental analysis and analyzed data. F.Z., H.S., and J.S. performed RNA-seq, MeRIP-seq, and analyzed the data. X.X., P.-Y.S., and P.W. performed inhibitor treatment and collected antiviral and cytotoxicity data. J.A.W. analyzed RNA-seq and MeRIP-seq data. Y.X., X.Y., and J.J. provided UNC0965, UNC0642, UNC1999, and MS1262 targeting G9a/Ezh2.

DECLARATION OF INTERESTS

X.C. is the founder of TransChromix, LLC. J.J. is a cofounder and equity shareholder in Cullgen, Inc., a scientific cofounder and scientific advisory board member of Onsero Therapeutics, Inc., and a consultant for Cullgen, Inc., EpiCypher, Inc., Accent Therapeutics, Inc, and Tavotek Biotherapeutics, Inc. The Jin laboratory received research funds from Celgene Corporation, Levo Therapeutics Inc., Cullgen, Inc. and Cullinan Oncology, Inc. The indication of using clinically trialed G9a/Ezh2 inhibitors for COVID-19 therapy is protected by US provisional patent application #63/113,211 as "Use of Method".

STAR★METHODS

Detailed methods are provided in the online version of this paper and include the following:

- KEY RESOURCES TABLE
- EXPERIMENTAL MODEL AND STUDY PARTICIPANT DETAILS
  - Cell lines and primary cultures of human origin
  - COVID-19 patient data
- METHOD DETAILS
  - Chemicals and reagents
  - SARS-CoV-2-Nluc antiviral assay
  - Cytotoxicity assay
  - m^6A RNA immunoprecipitation sequencing (m6A/MeRIP-seq) and data analysis
  - ChaC pull-down with biotin-conjugated inhibitors UNC0965 and UNC2399
  - Proteomics sample preparation
  - LC-MS/MS analysis details parameters
- QUANTIFICATION AND STATISTICAL ANALYSIS
  - Raw proteomics data processing and analysis
  - Analysis of functional category and networks

SUPPLEMENTAL INFORMATION

Supplemental information can be found online at https://doi.org/10.1016/j.isci.2025.112632.

Received: June 18, 2024
Revised: December 30, 2024
Accepted: May 7, 2025
Published: May 11, 2025

REFERENCES

1. Dong, E., Du, H., and Gardner, L. (2020). An interactive web-based dashboard to track COVID-19 in real time. Lancet Infect. Dis. *20*, 533–534.
2. Paranjpe, I., Russak, A.J., De Freitas, J.K., Lala, A., Miotto, R., Vaid, A., Johnson, K.W., Danieletto, M., Golden, E., Meyer, D., et al. (2020). Clinical Characteristics of Hospitalized Covid-19 Patients in New York City. Preprint at medRxiv. https://doi.org/10.1101/2020.04.19.20062117.
3. Menon, R., Otto, E.A., Sealfon, R., Nair, V., Wong, A.K., Theesfeld, C.L., Chen, X., Wang, Y., Boppanna, A., Luo, J., et al. (2020). SARS-CoV-2 receptor networks in diabetic kidney disease, BK-Virus nephropathy and COVID-19 associated acute kidney injury. Preprint at medRxiv. https://doi.org/10.1101/2020.05.09.20096511.
4. Sugiyama, K., Suzuki, C., Aoyama, M., Toyota, N., Nakagawa, N., Shozu, M., Nakai, K., and Iwano, K. (2022). Long-term observation of antibody titers against SARS-CoV-2 following vaccination. Public Health Pract. *4*, 100297.
5. Ishizaki, A., Bi, X., Nguyen, Q.T., Maeno, T., Hara, A., Nakamura, H., Kuramoto, S., Nishi, K., Ooe, H., and Ichimura, H. (2022). Neutralizing-antibody response to SARS-CoV-2 for 12 months after the COVID-19 workplace outbreaks in Japan. PLoS One *17*, e0273712.
6. Amicone, M., Borges, V., Alves, M.J., Isidro, J., Zé-Zé, L., Duarte, S., Vieira, L., Guiomar, R., Gomes, J.P., and Gordo, I. (2022). Mutation rate of SARS-CoV-2 and emergence of mutators during experimental evolution. Evol. Med. Public Health *10*, 142–155.
7. Abavisani, M., Rahimian, K., Mahdavi, B., Tokhanbigli, S., Mollapour Siasakht, M., Farhadi, A., Kodori, M., Mahmanzar, M., and Meshkat, Z. (2022). Mutations in SARS-CoV-2 structural proteins: a global analysis. Virol. J. *19*, 220–319.
8. Zhu, K.L., Jiang, X.L., Zhan, B.D., Wang, X.J., Xia, X., Cao, G.P., Sun, W. K., Huang, P.X., Zhang, J.Z., Gao, Y.L., et al. (2023). Durability of neutralization against Omicron subvariants after vaccination and breakthrough infection. Cell Rep. *42*, 112075. https://doi.org/10.1016/j.celrep.2023.112075.
9. Cox, M., Peacock, T.P., Harvey, W.T., Hughes, J., Wright, D.W., Willett, B.J., Thomson, E., Gupta, R.K., Peacock, S.J., et al.; COVID-19 Genomics UK COG-UK Consortium (2023). SARS-CoV-2 variant evasion of monoclonal antibodies based on in vitro studies. Nat. Rev. Microbiol. *21*, 112–124.
10. Gutlapalli, S.D., Ganipineni, V.D.P., Danda, S., Fabian, D., Okorie, I.J., Paramsothy, J., Kailayanathan, T., Umyarova, R., Aviles, C., Garlapati, S.K.P., et al. (2023). Exploring the Potential of Broadly Neutralizing Antibodies for Treating SARS-CoV-2 Variants of Global Concern in 2023: A Comprehensive Clinical Review. Cureus *15*, e36809.
11. Alcantara, M.C., Higuchi, Y., Kirita, Y., Matoba, S., and Hoshino, A. (2023). Deep Mutational Scanning to Predict Escape from Bebtelovimab in SARS-CoV-2 Omicron Subvariants. Vaccines *11*, 711.
12. Heilmann, E., Costacurta, F., Moghadasi, S.A., Ye, C., Pavan, M., Bassani, D., Volland, A., Ascher, C., Weiss, A.K.H., and Bante, D. (2022). SARS-CoV-2 3CLpro mutations selected in a VSV-based system confer resistance to nirmatrelvir, ensitrelvir, and GC376. Sci. Transl. Med. *15*, eabq7360.
13. Gandhi, S., Klein, J., Robertson, A.J., Peña-Hernández, M.A., Lin, M.J., Roychoudhury, P., Lu, P., Fournier, J., Ferguson, D., Mohamed Bakhash,

S.A.K., et al. (2022). De novo emergence of a remdesivir resistance mutation during treatment of persistent SARS-CoV-2 infection in an immunocompromised patient: a case report. Nat. Commun. *13*, 1547.

14. Hu, Y., Lewandowski, E.M., Tan, H., Zhang, X., Morgan, R.T., Zhang, X., Jacobs, L.M.C., Butler, S.G., Gongora, M.V., Choy, J., et al. (2022). Naturally occurring mutations of SARS-CoV-2 main protease confer drug resistance to nirmatrelvir. Preprint at bioRxiv. https://doi.org/10.1101/2022.06.28.497978.

15. Gavriilaki, E., and Kokoris, S. (2022). COVID-19 sequelae: can long-term effects be predicted? Lancet Infect. Dis. *22*, 1651–1652. https://doi.org/10.1016/S1473-3099(22)00529-1.

16. Lineburg, K.E., and Smith, C. (2023). The Persistence of SARS-CoV-2 and Its Role in Long Covid. NEJM Evid. *2*, EVIDe2300165. https://doi.org/10.1056/EVIDe2300165.

17. Diao, B., Wang, C., Tan, Y., Chen, X., Liu, Y., Ning, L., Chen, L., Li, M., Liu, Y., Wang, G., et al. (2020). Reduction and Functional Exhaustion of T Cells in Patients With Coronavirus Disease 2019 (COVID-19). Front. Immunol. *11*, 827. https://doi.org/10.3389/fimmu.2020.00827.

18. Liao, M., Liu, Y., Yuan, J., Wen, Y., Xu, G., Zhao, J., Cheng, L., Li, J., Wang, X., Wang, F., et al. (2020). Single-cell landscape of bronchoalveolar immune cells in patients with COVID-19. Nat. Med. *26*, 842–844. https://doi.org/10.1038/s41591-020-0901-9.

19. Liu, D., Wang, Q., Zhang, H., Cui, L., Shen, F., Chen, Y., Sun, J., Gan, L., Sun, J., Wang, J., et al. (2020). Viral sepsis is a complication in patients with Novel Corona Virus Disease (COVID-19). Med. Drug Discov. *8*, 100057.

20. Swenson, K.E., and Swenson, E.R. (2021). Pathophysiology of acute respiratory distress syndrome and COVID-19 lung injury. Crit. Care Clin. *37*, 749–776.

21. Wei, J., Alfajaro, M.M., DeWeirdt, P.C., Hanna, R.E., Lu-Culligan, W.J., Cai, W.L., Strine, M.S., Zhang, S.-M., Graziano, V.R., and Schmitz, C. O. (2020). Genome-wide CRISPR screens reveal host factors critical for SARS-CoV-2 infection. Cell *184*, 76–91.e13.

22. Ramlall, V., Thangaraj, P.M., Meydan, C., Foox, J., Butler, D., Kim, J., May, B., De Freitas, J.K., Glicksberg, B.S., Mason, C.E., et al. (2020). Immune complement and coagulation dysfunction in adverse outcomes of SARS-CoV-2 infection. Nat. Med. *26*, 1609–1615. https://doi.org/10.1038/s41591-020-1021-2.

23. Wang, L., Muneer, A., Xie, L., Zhang, F., Wu, B., Mei, L., Lenarcic, E.M., Feng, E.H., Song, J., Xiong, Y., et al. (2020). Novel gene-specific translation mechanism of dysregulated, chronic inflammation reveals promising, multifaceted COVID-19 therapeutics. Preprint at bioRxiv. https://doi.org/10.1101/2020.11.14.382416.

24. Muneer, A. (2023). Non-Canonical Translation Regulatory Function of G9a in Chronic Inflammation Associated Diseases (The University of North Carolina at Chapel Hill).

25. Sakai, M., Masuda, Y., Tarumoto, Y., Aihara, N., Tsunoda, Y., Iwata, M., Kamiya, Y., Komorizono, R., Noda, T., Yusa, K., et al. (2023). Genome-scale CRISPR–Cas9 screen identifies novel host factors as potential therapeutic targets for SARS-CoV-2 infection. Preprint at bioRxiv. https://doi.org/10.1101/2023.03.06.531431.

26. Malovannaya, A., Lanz, R.B., Jung, S.Y., Bulynko, Y., Le, N.T., Chan, D. W., Ding, C., Shi, Y., Yucer, N., Krenciute, G., et al. (2011). Analysis of the human endogenous coregulator complexome. Cell *145*, 787–799. https://doi.org/10.1016/j.cell.2011.05.006.

27. Huttlin, E.L., Ting, L., Bruckner, R.J., Gebreab, F., Gygi, M.P., Szpyt, J., Tam, S., Zarraga, G., Colby, G., Baltier, K., et al. (2015). The BioPlex Network: A Systematic Exploration of the Human Interactome. Cell *162*, 425–440. https://doi.org/10.1016/j.cell.2015.06.043.

28. Merad, M., and Martin, J.C. (2020). Pathological inflammation in patients with COVID-19: a key role for monocytes and macrophages. Nat. Rev. Immunol. *20*, 355–362. https://doi.org/10.1038/s41577-020-0331-4.

29. Wrobel, J.A., Xie, L., Wang, L., Liu, C., Rashid, N., Gallagher, K.K., Xiong, Y., Konze, K.D., Jin, J., Gatza, M.L., and Chen, X. (2019). Multi-omic Dissection of Oncogenically Active Epiproteomes Identifies Drivers of Proliferative and Invasive Breast Tumors. iScience *17*, 359–378. https://doi.org/10.1016/j.isci.2019.07.001.

30. Muneer, A., Wang, L., Xie, L., Zhang, F., Wu, B., Mei, L., Lenarcic, E.M., Feng, E.H., Song, J., Xiong, Y., et al. (2023). Non-canonical function of histone methyltransferase G9a in the translational regulation of chronic inflammation. Cell Chem. Biol. *30*, 1525–1541.e7. https://doi.org/10.1016/j.chembiol.2023.09.012.

31. Nie, X., Qian, L., Sun, R., Huang, B., Dong, X., Xiao, Q., Zhang, Q., Lu, T., Yue, L., Chen, S., et al. (2021). Multi-organ proteomic landscape of COVID-19 autopsies. Cell *184*, 775–791.e14. https://doi.org/10.1016/j.cell.2021.01.004.

32. Zhou, Y., Liu, Y., Gupta, S., Paramo, M.I., Hou, Y., Mao, C., Luo, Y., Judd, J., Wierbowski, S., Bertolotti, M., et al. (2023). A comprehensive SARS-CoV-2-human protein-protein interactome reveals COVID-19 pathobiology and potential host therapeutic targets. Nat. Biotechnol. *41*, 128–139. https://doi.org/10.1038/s41587-022-01474-0.

33. Zhao, B.S., Roundtree, I.A., and He, C. (2017). Post-transcriptional gene regulation by mRNA modifications. Nat. Rev. Mol. Cell Biol. *18*, 31–42. https://doi.org/10.1038/nrm.2016.132.

34. Roundtree, I.A., Evans, M.E., Pan, T., and He, C. (2017). Dynamic RNA Modifications in Gene Expression Regulation. Cell *169*, 1187–1200. https://doi.org/10.1016/j.cell.2017.05.045.

35. Meng, Y., Zhang, Q., Wang, K., Zhang, X., Yang, R., Bi, K., Chen, W., and Diao, H. (2021). RBM15-mediated N6-methyladenosine modification affects COVID-19 severity by regulating the expression of multitarget genes. Cell Death Dis. *12*, 732–810.

36. Sun, L., Li, P., Ju, X., Rao, J., Huang, W., Ren, L., Zhang, S., Xiong, T., Xu, K., Zhou, X., et al. (2021). In vivo structural characterization of the SARS-CoV-2 RNA genome identifies host proteins vulnerable to repurposed drugs. Cell *184*, 1865–1883.e20.

37. Zhang, X., Hao, H., Ma, L., Zhang, Y., Hu, X., Chen, Z., Liu, D., Yuan, J., Hu, Z., and Guan, W. (2021). Methyltransferase-like 3 modulates severe acute respiratory syndrome coronavirus-2 RNA N6-methyladenosine modification and replication. mBio *12*, e0106721.

38. Kumar, R., Khandelwal, N., Chander, Y., Nagori, H., Verma, A., Barua, A., Godara, B., Pal, Y., Gulati, B.R., Tripathi, B.N., et al. (2022). S-adenosylmethionine-dependent methyltransferase inhibitor DZNep blocks transcription and translation of SARS-CoV-2 genome with a low tendency to select for drug-resistant viral variants. Antiviral Res. *197*, 105232.

39. Qiu, X., Hua, X., Li, Q., Zhou, Q., and Chen, J. (2021). m6A Regulator-Mediated Methylation Modification Patterns and Characteristics of Immunity in Blood Leukocytes of COVID-19 Patients. Front. Immunol. *12*, 774776.

40. Qing, X., Chen, Q., and Wang, K. (2022). m6A regulator-mediated methylation modification patterns and characteristics in COVID-19 patients. Front. Public Health *10*.

41. Lu, L., Li, Y., Ao, X., Huang, J., Liu, B., Wu, L., and Li, D. (2022). The risk of COVID-19 can be predicted by a nomogram based on m6A-related genes. Infect. Genet. Evol. *106*, 105389.

42. An, S., Xie, Z., Liao, Y., Jiang, J., Dong, W., Yin, F., Li, W.-X., Ye, L., Lin, J., and Liang, H. (2022). Systematic analysis of clinical relevance and molecular characterization of m6A in COVID-19 patients. Genes Dis. *9*, 1170–1173.

43. Yi, Y., Li, Y., Meng, Q., Li, Q., Li, F., Lu, B., Shen, J., Fazli, L., Zhao, D., Li, C., et al. (2021). A PRC2-independent function for EZH2 in regulating rRNA 2'-O methylation and IRES-dependent translation. Nat. Cell Biol. *23*, 341–354. https://doi.org/10.1038/s41556-021-00653-6.

44. Bojkova, D., Klann, K., Koch, B., Widera, M., Krause, D., Ciesek, S., Cinatl, J., and Münch, C. (2020). Proteomics of SARS-CoV-2-infected

host cells reveals therapy targets. Nature *583*, 469–472. https://doi.org/10.1038/s41586-020-2332-7.

45. Liu, J., Xu, Y.P., Li, K., Ye, Q., Zhou, H.Y., Sun, H., Li, X., Yu, L., Deng, Y. Q., Li, R.T., et al. (2021). The m(6)A methylome of SARS-CoV-2 in host cells. Cell Res. *31*, 404–414. https://doi.org/10.1038/s41422-020-00465-7.
46. Burgess, H.M., Depledge, D.P., Thompson, L., Srinivas, K.P., Grande, R. C., Vink, E.I., Abebe, J.S., Blackaby, W.P., Hendrick, A., Albertella, M.R., et al. (2021). Targeting the m(6)A RNA modification pathway blocks SARS-CoV-2 and HCoV-OC43 replication. Genes Dev. *35*, 1005–1019. https://doi.org/10.1101/gad.348320.121.
47. Xie, L., Sheehy, R.N., Xiong, Y., Muneer, A., Wrobel, J.A., Park, K.-S., Velez, J., Liu, J., Luo, Y.-J., and Li, Y.-D. (2023). Novel brain-penetrant inhibitor of G9a methylase blocks Alzheimer disease proteopathology for precision medication. Preprint at medRxiv. *23297491*. https://doi.org/10.1101/2023.10.25.23297491.
48. Ankney, J.A., Muneer, A., and Chen, X. (2018). Relative and absolute quantitation in mass spectrometry–based proteomics. Annu. Rev. Anal. Chem. *11*, 49–77.
49. Konze, K.D., Ma, A., Li, F., Barsyte-Lovejoy, D., Parton, T., Macnevin, C. J., Liu, F., Gao, C., Huang, X.P., Kuznetsova, E., et al. (2013). An orally bioavailable chemical probe of the Lysine Methyltransferases EZH2 and EZH1. ACS Chem. Biol. *8*, 1324–1334. https://doi.org/10.1021/cb400133j.
50. Gordon, D.E., Jang, G.M., Bouhaddou, M., Xu, J., Obernier, K., White, K. M., O'Meara, M.J., Rezelj, V.V., Guo, J.Z., Swaney, D.L., et al. (2020). A SARS-CoV-2 protein interaction map reveals targets for drug repurposing. Nature *583*, 459–468.
51. Samavarchi-Tehrani, P., Abdouni, H., Knight, J.D., Astori, A., Samson, R., Lin, Z.-Y., Kim, D.-K., Knapp, J.J., St-Germain, J., and Go, C.D. (2020). A SARS-CoV-2-host proximity interactome. Preprint at bioRxiv. https://doi.org/10.1101/2020.09.03.282103.
52. Laurent, E.M., Sofianatos, Y., Komarova, A., Gimeno, J.-P., Tehrani, P. S., Kim, D.-K., Abdouni, H., Duhamel, M., Cassonnet, P., and Knapp, J. J. (2020). Global BioID-based SARS-CoV-2 proteins proximal interactome unveils novel ties between viral polypeptides and host factors involved in multiple COVID19-associated mechanisms. Preprint at bioRxiv. https://doi.org/10.1101/2020.08.28.272955.
53. Arunachalam, P.S., Wimmers, F., Mok, C.K.P., Perera, R.A.P.M., Scott, M., Hagan, T., Sigal, N., Feng, Y., Bristow, L., Tak-Yin Tsang, O., et al. (2020). Systems biological assessment of immunity to mild versus severe COVID-19 infection in humans. Science *369*, 1210–1220.
54. Carvelli, J., Demaria, O., Vély, F., Batista, L., Benmansour, N.C., Fares, J., Carpentier, S., Thibult, M.-L., Morel, A., and Remark, R. (2020). Association of COVID-19 inflammation with activation of the C5a–C5aR1 axis. Nature, 1–9.
55. Tay, M.Z., Poh, C.M., Rénia, L., MacAry, P.A., and Ng, L.F. (2020). The trinity of COVID-19: immunity, inflammation and intervention. Nat. Rev. Immunol., 1–12.
56. Kee, J., Thudium, S., Renner, D.M., Glastad, K., Palozola, K., Zhang, Z., Li, Y., Lan, Y., Cesare, J., Poleshko, A., et al. (2022). SARS-CoV-2 disrupts host epigenetic regulation via histone mimicry. Nature *610*, 381–388.
57. Wang, R., Lee, J.-H., Kim, J., Xiong, F., Hasani, L.A., Shi, Y., Simpson, E. N., Zhu, X., Chen, Y.-T., Shivshankar, P., et al. (2023). SARS-CoV-2 restructures host chromatin architecture. Nat. Microbiol. *8*, 679–694.
58. Hu, S., Song, Y., Zhou, Y., Jiao, Y., and Li, G. (2022). METTL3 Accelerates Breast Cancer Progression via Regulating EZH2 m6A Modification. J. Healthc. Eng. *2022*, 5794422.
59. Li, J., Guo, M., Tian, X., Wang, X., Yang, X., Wu, P., Liu, C., Xiao, Z., Qu, Y., and Yin, Y. (2020). Virus-Host Interactome and Proteomic Survey Reveal Potential Virulence Factors Influencing SARS-CoV-2 Pathogenesis. Med *2*, 99–112.e7.
60. Gordon, D.E., Hiatt, J., Bouhaddou, M., Rezelj, V.V., Ulferts, S., Braberg, H., Jureka, A.S., Obernier, K., Guo, J.Z., and Batra, J. (2020). Comparative host-coronavirus protein interaction networks reveal pan-viral disease mechanisms. Science *370*, eabe9403.
61. Straining, R., and Eighmy, W. (2022). Tazemetostat: EZH2 Inhibitor. J. Adv. Pract. Oncol. *13*, 158–163. https://doi.org/10.6004/jadpro.2022.13.2.7.
62. Han, H., Yang, L., Liu, R., Liu, F., Wu, K.-l., Li, J., Liu, X.-H., and Zhu, C.-l. (2020). Prominent changes in blood coagulation of patients with SARS-CoV-2 infection. Clin. Chem. Lab. Med. *58*, 1116–1120.
63. Liu, J., Li, Y., Liu, Q., Yao, Q., Wang, X., Zhang, H., Chen, R., Ren, L., Min, J., Deng, F., et al. (2021). SARS-CoV-2 cell tropism and multiorgan infection. Cell Discov. *7*, 17–24.
64. Klann, K., Bojkova, D., Tascher, G., Ciesek, S., Münch, C., and Cinatl, J. (2020). Growth factor receptor signaling inhibition prevents SARS-CoV-2 replication. Mol. Cell *80*, 164–174.e4.
65. Bouhaddou, M., Memon, D., Meyer, B., White, K.M., Rezelj, V.V., Correa Marrero, M., Polacco, B.J., Melnyk, J.E., Ulferts, S., Kaake, R.M., et al. (2020). The Global Phosphorylation Landscape of SARS-CoV-2 Infection. Cell *182*, 685–712.e19. https://doi.org/10.1016/j.cell.2020.06.034.
66. Stukalov, A., Girault, V., Grass, V., Bergant, V., Karayel, O., Urban, C., Haas, D.A., Huang, Y., Oubraham, L., and Wang, A. (2020). Multi-level proteomics reveals host-perturbation strategies of SARS-CoV-2 and SARS-CoV. Preprint at bioRxiv. https://doi.org/10.1101/2020.06.17.156455.
67. Kaneko, T., Esmail, S., Voss, C., Martin, C., Slessarev, M., Hovey, O., Ye, M., Kim, S., Fraser, D., and Li, S. (2021). System-wide hematopoietic and immune signaling aberrations in COVID-19 revealed by deep proteome and phosphoproteome analysis. Preprint at medRxiv. https://doi.org/10.1101/2021.03.19.21253675.
68. Su, Y., Chen, D., Yuan, D., Lausted, C., Choi, J., Dai, C.L., Voillet, V., Duvvuri, V.R., Scherler, K., Troisch, P., et al. (2020). Multi-omics resolves a sharp disease-state shift between mild and moderate COVID-19. Cell *183*, 1479–1495.e20.
69. Su, Y., Yuan, D., Chen, D.G., Ng, R.H., Wang, K., Choi, J., Li, S., Hong, S., Zhang, R., Xie, J., et al. (2022). Multiple early factors anticipate post-acute COVID-19 sequelae. Cell *185*, 881–895.e20.
70. Yaron, T.M., Heaton, B.E., Levy, T.M., Johnson, J.L., Jordan, T.X., Cohen, B.M., Kerelsky, A., Lin, T.-Y., Liberatore, K.M., and Bulaon, D.K. (2020). The FDA-approved drug Alectinib compromises SARS-CoV-2 nucleocapsid phosphorylation and inhibits viral infection in vitro. Preprint at bioRxiv. https://doi.org/10.1101/2020.08.14.251207.
71. Davidson, A.D., Williamson, M.K., Lewis, S., Shoemark, D., Carroll, M.W., Heesom, K.J., Zambon, M., Ellis, J., Lewis, P.A., Hiscox, J.A., and Matthews, D.A. (2020). Characterisation of the transcriptome and proteome of SARS-CoV-2 reveals a cell passage induced in-frame deletion of the furin-like cleavage site from the spike glycoprotein. Genome Med. *12*, 15–68.
72. Liu, S., Zhuo, L., Wang, J., Zhang, Q., Li, Q., Li, G., Yan, L., Jin, T., Pan, T., Sui, X., et al. (2020). METTL3 plays multiple functions in biological processes. Am. J. Cancer Res. *10*, 1631–1646.
73. Lin, S., Choe, J., Du, P., Triboulet, R., and Gregory, R.I. (2016). The m6A methyltransferase METTL3 promotes translation in human cancer cells. Mol. Cell *62*, 335–345.
74. Li, N., Hui, H., Bray, B., Gonzalez, G.M., Zeller, M., Anderson, K.G., Knight, R., Smith, D., Wang, Y., Carlin, A.F., and Rana, T.M. (2021). METTL3 regulates viral m6A RNA modification and host cell innate immune responses during SARS-CoV-2 infection. Cell Rep. *35*, 109091.
75. Malbec, L., Celerier, M., Bizet, M., Calonne, E., Hofmann-Winkler, H., Boeckx, B., Abdelnabi, R., Putmans, P., Hassabi, B., and Naesens, L. (2022). The RNA demethylase FTO controls m6A marking on SARS-CoV-2 and classifies COVID-19 severity in patients. Preprint at bioRxiv. 497749. https://doi.org/10.1101/2022.06.27.497749.

76. Gu, X., Wang, S., Zhang, W., Li, C., Guo, L., Wang, Z., Li, H., Zhang, H., Zhou, Y., Liang, W., et al. (2023). Probing long COVID through a proteomic lens: a comprehensive two-year longitudinal cohort study of hospitalised survivors. EBioMedicine *98*, 104851.

77. Park, J., Kim, H., Kim, S.Y., Kim, Y., Lee, J.-S., Dan, K., Seong, M.-W., and Han, D. (2020). In-depth blood proteome profiling analysis revealed distinct functional characteristics of plasma proteins between severe and non-severe COVID-19 patients. Sci. Rep. *10*, 22418.

78. Shen, B., Yi, X., Sun, Y., Bi, X., Du, J., Zhang, C., Quan, S., Zhang, F., Sun, R., Qian, L., et al. (2020). Proteomic and Metabolomic Characterization of COVID-19 Patient Sera. Cell *182*, 59–72.e15. https://doi.org/10.1016/j.cell.2020.05.032.

79. Wang, R., Simoneau, C.R., Kulsuptrakul, J., Bouhaddou, M., Travisano, K.A., Hayashi, J.M., Carlson-Stevermer, J., Zengel, J.R., Richards, C. M., Fozouni, P., et al. (2021). Genetic screens identify host factors for SARS-CoV-2 and common cold coronaviruses. Cell *184*, 106–119.e14.

80. Zhu, Y., Feng, F., Hu, G., Wang, Y., Yu, Y., Zhu, Y., Xu, W., Cai, X., Sun, Z., Han, W., et al. (2021). A genome-wide CRISPR screen identifies host factors that regulate SARS-CoV-2 entry. Nat. Commun. *12*, 961–1011.

81. Daniloski, Z., Jordan, T.X., Wessels, H.-H., Hoagland, D.A., Kasela, S., Legut, M., Maniatis, S., Mimitou, E.P., Lu, L., Geller, E., et al. (2021). Identification of required host factors for SARS-CoV-2 infection in human cells. Cell *184*, 92–105.e16.

82. Schneider, W.M., Luna, J.M., Hoffmann, H.-H., Sánchez-Rivera, F.J., Leal, A.A., Ashbrook, A.W., Le Pen, J., Ricardo-Lax, I., Michailidis, E., Peace, A., et al. (2021). Genome-scale identification of SARS-CoV-2 and pan-coronavirus host factor networks. Cell *184*, 120–132.e14.

83. Meganck, R.M., and Baric, R.S. (2021). Developing therapeutic approaches for twenty-first-century emerging infectious viral diseases. Nat. Med. *27*, 401–410.

84. Krause, P.R., Fleming, T.R., Longini, I.M., Peto, R., Briand, S., Heymann, D.L., Beral, V., Snape, M.D., Rees, H., Ropero, A.-M., et al. (2021). SARS-CoV-2 variants and vaccines. N. Engl. J. Med. *385*, 179–186.

85. Zhao, T.V., Hu, Z., Ohtsuki, S., Jin, K., Wu, B., Berry, G.J., Frye, R.L., Goronzy, J.J., and Weyand, C.M. (2022). Hyperactivity of the CD155 immune checkpoint suppresses anti-viral immunity in patients with coronary artery disease. Nat. Cardiovasc. Res. *1*, 634–648.

86. Menachery, V.D., Eisfeld, A.J., Schäfer, A., Josset, L., Sims, A.C., Proll, S., Fan, S., Li, C., Neumann, G., and Tilton, S.C. (2014). Pathogenic influenza viruses and coronaviruses utilize similar and contrasting approaches to control interferon-stimulated gene responses. mBio *5*, e01174-01114.

87. Izadpanah, A., Rappaport, J., and Datta, P.K. (2022). Epitranscriptomics of SARS-CoV-2 infection. Front. Cell Dev. Biol. *10*, 849298.

88. Ayaz, S., and Crea, F. (2020). Targeting SARS-CoV-2 using polycomb inhibitors as antiviral agents. Future Medicine.

89. Bergant, V., Yamada, S., Grass, V., Tsukamoto, Y., Lavacca, T., Krey, K., Mühlhofer, M.T., Wittmann, S., Ensser, A., Herrmann, A., et al. (2022). Attenuation of SARS-CoV-2 replication and associated inflammation by concomitant targeting of viral and host cap 2'-O-ribose methyltransferases. EMBO J. *41*, e111608.

90. Wan, L., Xu, K., Wei, Y., Zhang, J., Han, T., Fry, C., Zhang, Z., Wang, Y.V., Huang, L., Yuan, M., et al. (2018). Phosphorylation of EZH2 by AMPK suppresses PRC2 methyltransferase activity and oncogenic function. Mol. Cell *69*, 279–291.e5.

91. Liu, J., Hu, X., Luo, K., Xiong, Y., Chen, L., Wang, Z., Inuzuka, H., Qian, C., Yu, X., Xie, L., et al. (2024). USP7-Based Deubiquitinase-Targeting Chimeras Stabilize AMPK. J. Am. Chem. Soc. *146*, 11507–11514.

92. Ge, X.-Y., Li, J.-L., Yang, X.-L., Chmura, A.A., Zhu, G., Epstein, J.H., Mazet, J.K., Hu, B., Zhang, W., Peng, C., et al. (2013). Isolation and characterization of a bat SARS-like coronavirus that uses the ACE2 receptor. Nature *503*, 535–538.

93. Zhou, H., Ji, J., Chen, X., Bi, Y., Li, J., Wang, Q., Hu, T., Song, H., Zhao, R., Chen, Y., et al. (2021). Identification of novel bat coronaviruses sheds light on the evolutionary origins of SARS-CoV-2 and related viruses. Cell *184*, 4380–4391.e14.

94. Wang, N., Li, S.-Y., Yang, X.-L., Huang, H.-M., Zhang, Y.-J., Guo, H., Luo, C.-M., Miller, M., Zhu, G., Chmura, A.A., et al. (2018). Serological evidence of bat SARS-related coronavirus infection in humans, China. Virol. Sin. *33*, 104–107.

95. Sacco, M.T., Bland, K.M., and Horner, S.M. (2022). WTAP targets the METTL3 m6A-methyltransferase complex to cytoplasmic hepatitis C virus RNA to regulate infection. J. Virol. *96*, e100922.

96. Kim, G.-W., and Siddiqui, A. (2021). Hepatitis B virus X protein recruits methyltransferases to affect cotranscriptional N6-methyladenosine modification of viral/host RNAs. Proc. Natl. Acad. Sci. USA *118*, e2019455118.

97. Zannella, C., Rinaldi, L., Boccia, G., Chianese, A., Sasso, F.C., De Caro, F., Franci, G., and Galdiero, M. (2021). Regulation of m6A methylation as a new therapeutic option against COVID-19. Pharmaceuticals *14*, 1135.

98. Hao, H., Hao, S., Chen, H., Chen, Z., Zhang, Y., Wang, J., Wang, H., Zhang, B., Qiu, J., Deng, F., and Guan, W. (2019). N 6-methyladenosine modification and METTL3 modulate enterovirus 71 replication. Nucleic Acids Res. *47*, 362–374.

99. Batista-Roche, J.L., Gómez-Gil, B., Lund, G., Berlanga-Robles, C.A., and García-Gasca, A. (2022). Global m6A RNA Methylation in SARS-CoV-2 Positive Nasopharyngeal Samples in a Mexican Population: A First Approximation Study. Epigenomes *6*, 16.

100. Dubey, S., Das, S., Ghosh, R., Dubey, M.J., Chakraborty, A.P., Roy, D., Das, G., Dutta, A., Santra, A., Sengupta, S., and Benito-León, J. (2023). The Effects of SARS-CoV-2 Infection on the Cognitive Functioning of Patients with Pre-Existing Dementia. J. Alzheimers Dis. Rep. *7*, 119–128.

101. Boutajangout, A., Frontera, J., Debure, L., Vedvyas, A., Faustin, A., and Wisniewski, T. (2021). Plasma biomarkers of neurodegeneration and neuroinflammation in hospitalized COVID-19 patients with and without new neurological symptoms. Alzheimer's Dement. *17*, e057892.

102. Xie, X., Muruato, A.E., Zhang, X., Lokugamage, K.G., Fontes-Garfias, C. R., Zou, J., Liu, J., Ren, P., Balakrishnan, M., Cihlar, T., et al. (2020). A nanoluciferase SARS-CoV-2 for rapid neutralization testing and screening of anti-infective drugs for COVID-19. Nat. Commun. *11*, 5214–5311.

103. Konze, K.D., Pattenden, S.G., Liu, F., Barsyte-Lovejoy, D., Li, F., Simon, J.M., Davis, I.J., Vedadi, M., and Jin, J. (2014). A chemical tool for in vitro and in vivo precipitation of lysine methyltransferase G9a. ChemMedChem *9*, 549–553.

104. Liu, F., Barsyte-Lovejoy, D., Li, F., Xiong, Y., Korboukh, V., Huang, X.-P., Allali-Hassani, A., Janzen, W.P., Roth, B.L., Frye, S.V., et al. (2013). Discovery of an in vivo chemical probe of the lysine methyltransferases G9a and GLP. J. Med. Chem. *56*, 8931–8942.

105. Bolger, A.M., Lohse, M., and Usadel, B. (2014). Trimmomatic: a flexible trimmer for Illumina sequence data. Bioinformatics *30*, 2114–2120.

106. Dobin, A., Davis, C.A., Schlesinger, F., Drenkow, J., Zaleski, C., Jha, S., Batut, P., Chaisson, M., and Gingeras, T.R. (2013). STAR: ultrafast universal RNA-seq aligner. Bioinformatics *29*, 15–21.

107. Li, H., Handsaker, B., Wysoker, A., Fennell, T., Ruan, J., Homer, N., Marth, G., Abecasis, G., and Durbin, R.; 1000 Genome Project Data Processing Subgroup (2009). The sequence alignment/map format and SAMtools. Bioinformatics *25*, 2078–2079.

108. Zhou, Y., Zhou, B., Pache, L., Chang, M., Khodabakhshi, A.H., Tanaseichuk, O., Benner, C., and Chanda, S.K. (2019). Metascape provides a biologist-oriented resource for the analysis of systems-level datasets. Nat. Commun. *10*, 1523.

109. Butler, D., Mozsary, C., Meydan, C., Foox, J., Rosiene, J., Shaiber, A., Danko, D., Afshinnekoo, E., MacKay, M., Sedlazeck, F.J., et al. (2021). Shotgun transcriptome, spatial omics, and isothermal profiling of

SARS-CoV-2 infection reveals unique host responses, viral diversification, and drug interactions. Nat. Commun. *12*, 1660–1717.

110. Park, J., Foox, J., Hether, T., Beheshti, A., Saravia-Butler, A., Singh, U., and Wurtele, E.S. (2021). Systemic tissue and cellular disruption from SARS-CoV-2 infection revealed in COVID-19 autopsies and spatial omics tissue maps. Preprint at bioRxiv. https://doi.org/10.1101/2021.03.08.434433.

111. Weng, Y.-L., Wang, X., An, R., Cassin, J., Vissers, C., Liu, Y., Liu, Y., Xu, T., Wang, X., Wong, S.Z.H., et al. (2018). Epitranscriptomic m6A regulation of axon regeneration in the adult mammalian nervous system. Neuron *97*, 313–325.e6.

112. Picelli, S., Faridani, O.R., Björklund, A.K., Winberg, G., Sagasser, S., and Sandberg, R. (2014). Full-length RNA-seq from single cells using Smart-seq2. Nat. Protoc. *9*, 171–181.

113. Wessel, D., and Flügge, U.I. (1984). A method for the quantitative recovery of protein in dilute solution in the presence of detergents and lipids. Anal. Biochem. *138*, 141–143.

STAR★METHODS

KEY RESOURCES TABLE

REAGENT or RESOURCE	SOURCE	IDENTIFIER
Antibodies		
m^6A polyclonal antibody	Synaptic Systems	Cat#202003
Bacterial and virus strains		
SARS-CoV-2-Nluc	Xie et al.[102]	N/A
Biological samples		
Covid19 patient PBMCs	RayBiotech Life	Cat# CoV-PBMC
Chemicals, peptides, and recombinant proteins		
DMEM	Gibco	Cat#11965092
DMEM, no phenol red	Gibco	Cat#21063029
RPMI-1640	Gibco	Cat#11875119
HEPES	Thermo Fisher	Cat#AAA1477718
FBS	Gibco	Cat#26140079
penicillin, and streptomycin	Gibco	Cat#15140122
Blasticidin S	Thermo Fisher	Cat#BP264725
L-glutaMax	Gibco	Cat#31-415-029
Sodium Pyruvate	Thermo Fisher	Cat#BP356-100
protease inhibitor cocktail	Sigma	Cat#P8340
PMSF	Acros Organics	Cat#215740100
Igepal CA630	Sigma	Cat#I3021
BCA assay kit	Thermo Fisher	Cat#23225
neutravidin-agarose	Thermo Fisher	Cat#29201
Sequence grade Trypsin	Promega	Cat#V511C
C18 (Octadecyl)	Empore 3M	Cat#2215
MS grade trifluoroacetic acid	Thermo-Fisher	Cat#85183
0.1% formic acid	Thermo-Fisher	Cat#LS118-212
ACN and 0.1% formic acid	Thermo-Fisher	Cat#LS120-1
UNC0965	Konze et al.[103]	N/A
UNC2399	Konze et al.[49]	N/A
UNC0642	Liu et al.[104]	N/A
UNC1999	Konze et al.[49]	N/A
MS1262	Xie et al.[47]	N/A
Tazemetostat	Selleck	Cat# S7128
TMT 11-plex Isobaric Labeling Reagent Kit	Thermo Fisher	Cat# A34808
TRIzol	Life Technologies	Cat# 10296010
Dynabeads Oligo $(dT)_{25}$	Thermo Fisher	Cat# 61006
Dynabeads Protein A	Thermo Fisher	Cat# 10001D
N^6-Methyladenosine	Sigma-Aldrich	Cat# M2780
RNase Inhibitor	NEB	Cat# M0314S
SMARTScribe reverse transcriptase	Takara	Cat# 639536
Advantage Polymerase Mix	Takara	Cat# 639201
AMPure XP beads	Fisher Scientific	Cat# A63880
EZ Tn5 Transposase	Lucigen	Cat# TNP92110
KAPA HiFi hotstart readymix	EMSCO/FISHER	Cat# KK2601
KAPA Library Quantification Kit	Fisher	Cat# NC0078468

(*Continued on next page*)

Continued

REAGENT or RESOURCE	SOURCE	IDENTIFIER
Critical commercial assays		
Cell Counting kit-8	Sigma	Cat# 96992
RNA Clean & Concentrator-5 kit	Zymo	Cat# R1015
High-Select™ Fe-NTA Phosphopeptide Enrichment Kit	Thermo Fisher	Cat#A32992
Deposited data		
MS proteomics data	This paper	PRIDE: PXD058743
RNA-Seq and MeRIP-Seq data	This paper	GEO: GSE282914
Experimental models: Cell lines		
Human: A549-hACE2	Invivogen	Cat# a549-hace2
Software and algorithms		
The R Project	The R Project	https://www.r-project.org/
MATLAB (R2017b)	Mathworks	https://www.mathworks.com/products/matlab.html
Cytoscape version 3.8.0	Cytoscape Consortium	https://cytoscape.org/
GraphPad Prism v8 & v9	GraphPad	https://www.graphpad.com/scientific-software/prism/
bcl2fastq2 v2.17.1.14	Illumina	https://github.com/igorbarinov/bcl2fastq
Trimmomatic-0.32 software	Bolger et al.[105]	https://github.com/usadellab/Trimmomatic
STAR v.2.7.6a	Dobin et al.[106]	https://github.com/alexdobin/STAR
SAMtools-1.1 software	Li et al.[107]	http://samtools.sourceforge.net/
Integrative Genomics Viewer (IGV)	Broad Institute	https://software.broadinstitute.org/software/igv/
UCSC Genome Browser	UCSC	https://genome.ucsc.edu/
Maxquant version 2.1.0.0	Maxquant	https://www.maxquant.org/maxquant/
Perseus version 1.6.10.50	Perseus	https://www.maxquant.org/perseus/
Ingenuity Pathway Analysis	Qiagen	https://digitalinsights.qiagen.com/products-overview/discovery-insights-portfolio/analysis-and-visualization/qiagen-ipa/
DAVID bioinfomatics	DAVID bioinfomatics	http://david.abcc.ncifcrf.gov/
Metascape	Zhou et al.[108]	https://metascape.org/
STRING	STRING	http://string-db.org/
Other		
Easy nanoLC 1200	Thermo Fisher	N/A
Q-Exactive HFX Orbitrap mass spectrometer	Thermo Fisher	N/A
NextSeq 550	Illumina	N/A
NanoLC trap column	SCIEX	Cat#5016752
Acclaim Pepmap C18 RP column	Thermo Fisher	Cat#164261

EXPERIMENTAL MODEL AND STUDY PARTICIPANT DETAILS

Cell lines and primary cultures of human origin

Human alveolar epithelial cells that overexpress hACE2 receptor (A549-hACE2) were maintained in high-glucose DMEM supplemented with 10% fetal bovine serum (FBS), 1% penicillin/streptomycin (P/S; 10,000 U/mL), 1% 4-(2-hydroxyethyl)-1-piperazineethanesulfonic acid (HEPES) and 10 μg/mL Blasticidin S. Peripheral blood mononuclear cells (PBMCs) isolated from patients with COVID-19 were purchased from RayBiotech Life (Peachtree Corners, GA) and were maintained in RPMI 1640 containing 10% FBS, 100 units/ml P/S, 2 mM L-glutaMax (Gibco), 10 mM HEPES and 1 mM Sodium Pyruvate at a density of 1.5×10^6 cells/ml. Patient PBMC related metadata (gender, age, disease severity, etc.) is provided in Table S6B. The cells were treated with UNC0642, MS1262, UNC1999 or TAZVERIK (Taz, Tazemetostat) at 1 μM for 0 to 48 h before being harvested for subsequent proteomic, RNA-seq, and molecular/cell biological studies. All cells were grown at 37°C in humidified air with 5% carbon dioxide and tested negative for mycoplasma.

COVID-19 patient data

Publicly available shotgun transcriptome (bulk RNA-seq), spatial omics (GeoMx), and isothermal profiling datasets along with associated metadata from dbGAP (accession #38851 and ID phs002258.v1.p1), GEO (GSE169504) and Mendeley (https://doi.org/10.17632/f4wh42nshy.2) were used to investigate changes in expression of G9a, EZH2, and METTL3 complex members (Figures S1A and S1B), and G9a/METTL3-coregulated m6A modified transcripts (Figure 5C) in naso/oropharyngeal swabs (n = 669) and autopsy samples (liver, kidney, heart, lung, lymph node) from COVID-19 patients (n = 39).[109,110] Additional information is provided in relevant figure legends. Processed bulk RNA-seq data is also available online for simple visualization and exploration of gene expression and enriched pathways (https://covidgenes.weill.cornell.edu/).[109,110]

METHOD DETAILS

Chemicals and reagents

Cell culture media, other components, and fetal bovine serum were obtained from Gibco/ThermoFisher. Trypsin was purchased from Promega. A549-hACE2 cell line was purchased from InvivoGen. All chemicals used during preparation of proteomic samples were HPLC-grade unless specifically indicated. Inhibitors (UNC0642, UNC1999 and MS1262) and probes (UNC0965, UNC2399) targeting G9a/Ezh2 were synthesized in Dr. Jian Jin's lab. Tazemetostat (Cat. S7128) was purchased from Selleck. TMT 11-plex isobaric labeling reagent kit was purchased from Thermo-Fisher (Cat. A34808).

SARS-CoV-2-Nluc antiviral assay

A549-hACE2 and SARS-CoV-2-Nluc were used for evaluating the compounds as described.[102] Briefly, A549-hACE2 cells (12,000 cells per well in phenol red-free medium containing 2% FBS) were plated into a white opaque 96-well plate (Corning). On the next day, 3-fold serial dilutions of compounds were prepared in DMSO. One microliter of compound was mixed with 99 μL of SARS-CoV-2-Nluc virus that was diluted in phenol red-free culture medium containing 2% FBS. Compound-virus mixtures (50 μL) were added to each well of the 96-well plates containing A549-hACE2 cells (MOI 0.025). At 48 h post-infection, 50 μL of Nanoluciferase substrates (Promega) were added to each well. Luciferase signals were measured using a Synergy Neo2 microplate reader (BioTek). The relative luciferase signals were calculated by normalizing the luciferase signals of the compound-treated groups to the signals of the DMSO-treated groups (set as 100%). The relative luciferase signal (Y-axis) versus the log10 values of compound concentration (X-axis) was plotted in software Prism 9. The EC_{50} (compound concentration for reducing 50% of luciferase signal) was calculated using a nonlinear regression model (four parameters). Two experiments were performed with technical duplicates.

Cytotoxicity assay

A549-hACE2 cells (5000 cells per well in phenol red-free medium containing 2% FBS) were plated into a clear flat-bottom 96-well plate (Nunc). On the next day, 3-fold serial dilutions of compounds were prepared in DMSO. The compounds were further diluted 100-fold. Diluted compound solutions (50 μL) were added to each well of the cell plates. At 72 h post-treatment, 4 μL of Cell Counting Kit-8 (CCK-8; Sigma-Aldrich) was added to each well. After incubation at 37°C for 90 min, absorbance at 450 nm was measured using the Cytation5 multi-mode microplate reader (BioTek). The relative cell viability was calculated by normalizing the absorbance of the compound-treated groups to the absorbance of the DMSO-treated groups (set as 100%). The relative cell viability (Y-axis) versus the log10 values of compound concentration (X-axis) were plotted in software Prism 8. The CC50 (compound concentration for reducing 50% of cell viability) was calculated using a nonlinear regression model (four parameters). Two experiments were performed with technical duplicates.

m^{6}A RNA immunoprecipitation sequencing (m6A/MeRIP-seq) and data analysis

The m^{6}A/MeRIP-Seq was performed as described with some modifications.[111] Briefly, total RNA was extracted from A549-hACE2 and patient PBMCs using TRIzol (Life Technologies) followed by purification using illustra^{TM} RNA spin Mini kit (GE Healthcare, UK). mRNA was isolated from 10 μg total RNA using Dynabeads Oligo $(dT)_{25}$ (Thermo Fisher; 61006) according to manufacturer's instructions. Ten percent of a total of 150 ng mRNA was used as input, while the rest was incubated with 3 μg anti-m^{6}A polyclonal antibody (Synaptic Systems; 202003) that was pre-conjugated to Dynabeads Protein A (Thermo Fisher; 10001D) in 500 μL IP buffer (50 mM Tris, pH 7.4, 150 mM NaCl, 0.1% Igepal CA-630) for 2 h at 4°C. After washing the beads twice with IP-buffer and twice with high-salt wash buffer (50 mM Tris pH 7.4, 500 mM NaCl, 0.1% Igepal CA-630) for 5 min each, the m^{6}A-tagged mRNA was eluted using 100 μL IP-buffer containing 6.7 mM N^6-Methyladenosine (Sigma-Aldrich; M2780) and 40 U RNase Inhibitor (NEB, M0314S) and then recovered with RNA Clean and Concentrator-5 spin columns (Zymo; R1015).

The input and m^{6}A-IPed mRNA were subjected to library generation using the SMART-seq protocol as described.[112] For first strand cDNA synthesis, the mRNA was mixed with 0.25 μL RNase inhibitor and 1 μL CDS primer (5′-AAGCAGTGGTATCAACGCAGAGTACT30VN-3′) and heated to 70°C for 2 min. Then the mixture containing 0.5 μL of 100 mM DTT, 0.3 μL of 200 mM $MgCl_2$, 1 μL of 10 mM dNTPs, 0.25 μL RNase inhibitor, 1 μL of 10 μM TSO primer (5′-AAGCAGTGGTATCAACGCAGAGTACATrGrGrG-3′), 2 μL of 5X SMARTScribe RT buffer and 0.5 μL SMARTScribe reverse transcriptase (Takara, 639536) was added to perform reverse transcription. The cDNA was then amplified by Advantage Polymerase Mix (TAKARA, 639201) with IS primer (5′-AAGCAGTGGTATCAACGCAGAGT-3′). After purification with 0.8X AMPure XP beads (Fisher Scientific, A63880), the fragmentation of 100 pg cDNA

was performed with EZ Tn5 Transposase (Lucigen, TNP92110). Fragments of cDNA were amplified by KAPA HiFi hotstart readymix (EMSCO/FISHER, KK2601) with the Nextera i7 primer and Nextera i5 primer. The DNA was purified with 0.8X AMPure XP beads and quantified by qPCR with KAPA Library Quantification Kit (Fisher, NC0078468). The DNA from different samples was pooled at equal molar amounts, and the final sequencing library was loaded at concentrations of 2.7 pM and sequenced on a NextSeq 550 (Illumina) for single-end sequencing.

Raw sequencing data were de-multiplexed using bcl2fastq2 v2.17.1.14 (Illumina) and adapters were removed using Trimmomatic-0.32 software. Then the Input and m6A-IP reads were mapped to a combined reference genome consisting of human (GRCh38/hg38) and Ensembl SARS-CoV-2 isolate Wuhan-Hu-1 genomes (Genome Assembly: ASM985889v3, Accession: GCA_009858895.3; Sequence: MN908947.3) using STAR v.2.7.6a. Only uniquely mapping reads at the exon level for each gene were quantified and summarized to gene counts. Differential gene expression analysis was performed using DESeq2 v.1.32.0. Resulting bam files were sorted and indexed using SAMtools v.1.1, and MACS2 v.2.2.7.1 was used for m^6A peak calling using the bam files for each m^6A-IP/input pair. The R packages GenomicRanges v1.36.1 and AnnotationHub v.3.4.0 were used to identify genes overlapping the peaks determined by MACS2, and CHIPseeker v.1.30.3 was used to create profile plots.

ChaC pull-down with biotin-conjugated inhibitors UNC0965 and UNC2399

ChaC pull-downs were conducted as described,[23] with a few modifications. Briefly, cell pellets were resuspended in extraction buffer (50 mM Tris-HCl at pH7.5, 150 mM NaCl, 0.5% IGPAL-CA630 and 1 mM PMSF) followed by brief sonication and centrifugation to collect supernatant. Cell lysate (1 mg) was incubated overnight at 4°C with 2 nmol UNC0965/UNC2399 pre-coupled to 50 μL neutravidin-agarose (Thermo-Fisher) and washed thrice with 1 mL extraction buffer to remove nonspecific proteins. For on-beads sampling and processing, five additional washes with wash buffer (50 mM Tris-HCl pH7.5, 150 mM NaCl, 1 mM PMSF) were used to remove residual detergents. On-beads tryptic digestion was performed with 100 μL buffer containing 2 M urea, 25 mM Tris-HCl pH8.0, 1 mM DTT, 400 ng trypsin (Promega) for 30 min at room temperature on a mixer (Eppendorf). Partial digests were collected, and beads eluted twice more with 100 μL elution buffer (2 M urea, 25 mM Tris-HCl pH8.0, 5 mM iodoacetamide), incubated for 30 min at room temperature with shaking. Combined eluates were acidified with trifluoroacetic acid at final concentration of 1% (TFA, mass spec grade, Thermo-Fisher) and desalted with homemade C18 stage tips.

Proteomics sample preparation

Patient PBMCs and A549-hACE2 cells were lysed in 2x Laemmli buffer followed by protein precipitation using a methanol-chloroform method.[113] The resulting supernatant was mixed with Trizol LS reagent (Invitrogen, Cat 10296010), and proteins were further isolated and precipitated following the manufacturer's instructions. Protein pellets were resuspended in 8 M urea, 50 mM Tris-HCl pH 8.0, reduced with dithiothreitol (5 mM final) for 30 min at room temperature, and alkylated with iodoacetamide (15 mM final) for 45 min in the dark at room temperature. Samples were diluted 4-fold with 25 mM Tris-HCl pH 8.0, 1 mM $CaCl_2$ and digested with trypsin at 1:100 (w/w, trypsin:protein) ratio overnight at ambient temperature. Peptides were desalted using homemade C18 stage tips, and their concentrations were determined (Peptide assay, Thermo 23275). The cleaned peptides were used for LC-MS analysis or for additional labeling.

For TMT-labeling, 100 μg of each peptide sample was used for labeling with isobaric stable tandem mass tags (TMT11, Thermo Fisher Scientific, San Jose, CA) following manufacture instruction. The mixture of labeled peptides was desalted on Cep-Pak light C18 cartridge (Waters). Phosphopeptides were enriched with High-Select Fe-NTA Phosphopeptide Enrichment Kit (Thermo Scientific). Non-phosphopeptides (100 μg) were fractionated into 24 fractions using C18 stage tips and 10 mM TMAB (pH 8.5) containing 5–50% acetonitrile.

For secretome studies, secreted proteins were isolated from mixtures of culture supernatant and Trizol LS reagent (Invitrogen, Cat 10296010) following manufacturer's instruction. Resulting protein pellets were solubilized in buffer containing 50 mM Tris (pH 8.0) and 8 M urea, then processed in the same way as that for proteome to obtain purified peptides. LFQ was used for protein quantification of secretome.

LC-MS/MS analysis details parameters

Dried peptides were dissolved in 30 μL of 0.1% formic acid, 2% acetonitrile. One microgram phosphopeptides or 0.5 μg non-phosphopeptides from each fraction was analyzed on a Q-Exactive HF-X coupled with an Easy nanoLC 1200 (Thermo Fisher Scientific, San Jose, CA). Peptides were loaded on to a nanoEase MZ HSS T3 Column (100 Å, 1.8 μm, 75 μm × 250 mm, Waters). Parameters for MS and LC are listed in Table S6A.

QUANTIFICATION AND STATISTICAL ANALYSIS

Raw proteomics data processing and analysis

Mass spectra were processed, and peptide identification/quantification performed using MaxQuant software version 2.1.0.0 (Max Planck Institute, Germany). All protein database searches were performed against the UniProt human protein sequence database (UP000005640). False discovery rates (FDR) for peptide-spectrum match (PSM) and protein assignment were set at 1%. Search parameters included up to two missed cleavages at Lys/Arg, oxidation of methionine, protein N-terminal acetylation and

phosphorylation on serine, threonine, and tyrosine as dynamic modifications. Carbamidomethylation of cysteine residues was considered as a static modification. Peptide identifications are reported by filtering of reverse and contaminant entries and assigning to their leading razor protein. Data processing and statistical analysis were performed using Perseus (Version 1.6.10.50). Protein quantitation was performed on biological replicates and a two-sample t-test statistic was used with a *p*-value of 5% to report statistically significant protein or phosphopeptide abundance fold-changes. LFQ was used during ChaC-MS (Figures 1B, 1C, and S1C–S1E), G9a/Ezh2-inhibitor treatment of COVID-19 patient PBMCs (5a & S6), and secretome studies (parts of Figures 2 and S2). All other experiments used TMT-labeling. To correct for batch/experiment effect, TMT intensities were normalized to the replicate with lowest total intensity (for global, phospho & secretome studies). ChaC-MS intensities were not normalized, as intensity is directly proportional to the strength of interaction with bait protein (instead empty/negative-probe controls were used to screen out false positives).

Analysis of functional category and networks

Canonical pathway, biological function and upstream regulator analyses were performed using IPA (https://www.ingenuity.com/), DAVID (http://david.abcc.ncifcrf.gov/), Metascape (https://metascape.org/), and STRING (http://string-db.org/). Figures were generated using RStudio and interactome analyses were performed in Cytoscape v3.8.0. When comparing two conditions (overall m6A-modification levels), Mann Whitney–U test was used. A p value ≤ 0.05 was considered as significant. When p values were depicted as asterisks the following applies: * <0.05; ** <0.01; *** <0.001; **** <0.0001. For other figures, the statistical test and exact p value used for calculating the significance of each graph is indicated in the figure legend.